

~~CONFIDENTIAL~~

RM A53G10

NACA RM A53G10



# RESEARCH MEMORANDUM

FLIGHT MEASUREMENTS OF THE HORIZONTAL-TAIL LOADS ON A  
SWEPT-WING FIGHTER AIRPLANE AT TRANSONIC SPEEDS

By Melvin Sadoff

Ames Aeronautical Laboratory  
Moffett Field, Calif.

CLASSIFICATION CHANGED

**LIBRARY COPY**

UNCLASSIFIED

NOV 10 1953

To.....

By authority of NACA Res also effective July 26, 1957 AMT 8-21-57 RN-118 date July 26, 1957

LANGLEY AERONAUTICAL LABORATORY  
LIBRARY, NACA  
LANGLEY FIELD, VIRGINIA

CLASSIFIED DOCUMENT

This material contains information affecting the National Defense of the United States within the meaning of the espionage laws, Title 18, U.S.C., Secs. 793 and 794, the transmission or revelation of which in any manner to an unauthorized person is prohibited by law.

## NATIONAL ADVISORY COMMITTEE FOR AERONAUTICS

WASHINGTON

November 6, 1953

~~CONFIDENTIAL~~



## NATIONAL ADVISORY COMMITTEE FOR AERONAUTICS

RESEARCH MEMORANDUMFLIGHT MEASUREMENTS OF THE HORIZONTAL-TAIL LOADS ON A  
SWEPT-WING FIGHTER AIRPLANE AT TRANSONIC SPEEDS

By Melvin Sadoff

## SUMMARY

Flight tests on a swept-wing fighter airplane at Mach numbers from 0.6 to about 1.03 at 35,000 feet have indicated the critical flight regions for balancing, maneuvering, and buffeting horizontal-tail loads.

The critical balancing tail loads were found to occur at the highest test Mach number of about 1.03 at the highest airplane load factor.

The maneuvering tail loads were critical at Mach numbers less than 0.90. The maximum maneuvering load was an up load experienced during recovery from a pitch-up maneuver initiated by a decrease in wing-fuselage stability with an increase in normal-force coefficient at a Mach number of about 0.87.

Maximum buffet tail-load increments were experienced at Mach numbers less than 0.85. These buffet-load increments were relatively small compared to the maximum balancing and maneuvering tail loads.

## INTRODUCTION

Measurements in flight of the horizontal-tail loads over a wide range of conditions are important to the structural designer for identifying critical flight regions for tail loads and for providing him with a check on the reliability of existing methods for estimating or computing design loads for the horizontal tail. Considerable information on flight-measured tail loads is available on straight-wing fighter airplanes at relatively low Mach numbers (e.g., refs. 1 to 4). References 5 and 6 present some flight measurements of tail loads at high subsonic speeds on two swept-wing research airplanes.

~~CONFIDENTIAL~~

The present paper presents additional tail-load information from flight tests of a 35° swept-wing fighter airplane at transonic speeds. Though these tests were conducted primarily to obtain stability and control characteristics (refs. 7 and 8), the flight limits of the test airplane with regard to Mach number and load factor for the balancing tail-load condition were reached at the test altitude of 35,000 feet. Maneuvering tail loads were available from abrupt elevator-pulse maneuvers performed to evaluate the dynamic stability characteristics of the test airplane. Maneuvering tail-load data were also obtained during pitch-ups where the pilot, abruptly applying corrective control to maintain constant load factor or to arrest the pitch-up, introduced maneuvering load increments on the horizontal tail. The tests were made at 35,000 feet to prevent inadvertent overloading of the wing and tail surfaces. The experimental data are extrapolated to design conditions at 35,000 feet as well as 12,000 feet to investigate critical loading conditions.

To provide an indication of the accuracy with which these loads may be predicted, comparisons are made with results computed from wind-tunnel and flight data.

#### SYMBOLS

$\bar{c}$	mean aerodynamic chord, ft
$C_N$	airplane normal-force coefficient, $\frac{W_n}{qS}$
$C_{m_{Ow+f}}$	wing-fuselage pitching-moment coefficient about airplane center of gravity at zero lift, $\frac{\text{moment}}{qS\bar{c}}$
$F_A$	load on horizontal-tail actuator, lb
$F_{C.B.}$	load on two horizontal-tail clevis bolts, lb
$F_e$	elevator control force, lb
$g$	acceleration of gravity, ft/sec <sup>2</sup>
$I_y$	pitching moment of inertia, slug-ft <sup>2</sup>
$L_t$	horizontal-tail load, lb
$l_t$	horizontal-tail length, distance between airplane center of gravity and horizontal-tail quarter chord, ft

M	Mach number
N	airplane normal force, lb
n	airplane load factor (N/W)
P/2	time to complete one-half cycle elevator motion, sec
q	dynamic pressure, lb/sq ft
S	wing area, sq ft
t	time, sec
W	airplane weight, lb
W <sub>t</sub>	horizontal-tail weight, lb
x	distance between airplane center of gravity and the chordwise center of pressure of additional load on the wing and fuselage, (positive when forward of center of gravity), ft
$\alpha$	angle of attack, deg
$\delta_e$	elevator angle, radians or degrees as noted
$\dot{\delta}_e$	elevator control rate, deg/sec
$\delta_s$	stabilizer angle, deg
$\dot{\theta}$	pitching velocity, radians/sec
$\ddot{\theta}$	pitching acceleration, radians/sec <sup>2</sup>
$\omega$	natural frequency of airplane short-period longitudinal oscillation, radians/sec
$\omega_1$	elevator control frequency $\left(\frac{\pi}{P/2}\right)$ , radians/sec
$\Delta$	before a symbol denotes change of quantity from an initial value

## Subscripts

w+f	wing-fuselage combination
T	total

A	aerodynamic
bal	balancing
t	tail
man	maneuvering
max	maximum value
meas	measured value
1	first-peak value in elevator-pulse maneuver
2	second-peak value in elevator-pulse maneuver

#### AIRPLANE AND INSTRUMENTATION

The test airplane is a jet-powered fighter with sweptback wing and tail surfaces. A photograph of the airplane in its flight-test configuration is presented in figure 1. A two-view drawing of the airplane is given in figure 2. The physical characteristics of the airplane are listed in table I.

Standard NACA instruments and an 18-channel oscillograph were used to record all measured quantities. The horizontal-tail loads were measured by means of strain gages at three pin-joined attachment fittings (two clevis bolts and the horizontal-tail actuator) which join the tail to the fuselage. The pertinent geometric characteristics of the horizontal tail are presented in figure 3. For simplicity, the outputs of the strain gages of the two clevis bolts were combined electrically to give a single resultant trace on the 18-channel oscillograph. Thus, only two channels were required to record the tail load. The aerodynamic and the total tail loads were obtained by the following relationships:

$$L_{t_{\text{meas}}} = F_A + F_{C.B.}$$

$$L_{t_A} = L_{t_{\text{meas}}} + (n - 1) W_t - \left( \frac{\ddot{\theta} l_t}{g} \right) W_t$$

$$L_{t_T} = L_{t_{\text{meas}}} - W_t$$

For simplicity the center of gravity of the tail was assumed at the quarter chord in the above equations.

Airplane angle of attack was measured by a vane mounted on a boom one tip-chord length ahead of the wing tip. Horizontal-tail angle-of-attack measurements were obtained at two spanwise stations (22- and 92-percent tail semispan) from vanes mounted one and one-half chord lengths ahead of the tail (fig. 2). The angles of attack recorded by the vanes mounted at the tips of the wing and tail were corrected for induced flow effects due to the presence of the wing and horizontal tail, respectively. The true Mach number was determined from the nose-boom airspeed system calibrated over the test Mach number range by the NACA radar-phototheodolite method as reported in reference 9.

#### TEST CONDITIONS

The center of gravity of the airplane for these tests was located at an average value of 22.5 percent of the mean aerodynamic chord (fuselage station 184.64). The average weight of the airplane, as flown, was approximately 12,400 pounds as compared with the design normal gross weight of 13,395 pounds and the design light weight of 10,288 pounds. Unless otherwise noted, the stabilizer setting was  $0.6^\circ$ . The automatic wing leading-edge slats remained closed during these tests.

#### Gradual Maneuvers

Balancing tail loads were obtained over a Mach number range of approximately 0.4 to 1.1 and over a load factor range of about 0 to 7 at 35,000 feet for all runs identified as gradual maneuvers in figure 4(a). Figures 4(a) and 4(b) also show the Mach number load-factor envelope at 35,000 feet and 12,000 feet, respectively, to indicate the design conditions to which the experimental results are extrapolated later. The data were measured in steady straight flight and in wind-up turns up to either the stall or the limit load factor of the tests. At Mach numbers up to 0.96, pitch-ups were experienced which were initiated by stability changes resulting either from increasing angle of attack at constant Mach number or from decreasing Mach number at constant angle of attack. (See ref. 8.) In these pitch-ups relatively large maneuvering load increments were obtained on the tail when the pilot applied abrupt corrective control. Up to Mach numbers of about 0.96, the elevator was used as the primary control for this phase of the tests. At higher Mach numbers, the movable stabilizer was used as the primary control.

## Abrupt Maneuvers

Tail loads were also measured in abrupt maneuvers over a Mach number range of 0.60 to 1.05 at 35,000 feet. (See fig. 4(a).) The data were measured in elevator-pulse maneuvers made, for convenience, to negative increments of load factor from an initial value of about 1. The maximum control deflections and control rates<sup>1</sup> used in the elevator-pulse maneuvers are presented in figures 5(a) and 5(b), respectively. It may be pointed out that these maximum deflections were positive or down increments corresponding to the push-down and recovery type of maneuver used. The control rates designated as first peak and second peak were positive and negative maximum rates corresponding to the push-down and the recovery phases, respectively, of the pulse maneuvers. The effective control frequencies,  $\omega_1$ , which are defined as the ratio of  $\pi$  to the time required to complete one-half cycle of elevator motion, are shown in figure 5(c) for the elevator-pulse maneuvers.

## Buffet Loads

The buffet boundary for the test airplane is included in figure 4(a) to indicate the flight range beyond this boundary for which the buffet tail loads were obtained during the tests described as gradual maneuvers.

## RESULTS AND DISCUSSION

### Balancing Tail Loads

The balancing tail load may be given as

$$(L_{tA})_{bal} = \frac{C_{m_{Ow+f}} q S \bar{c}}{x + l_t} + \frac{nWx}{x + l_t}$$

where  $x$  is the distance between the chordwise center of pressure of additional load on the wing-fuselage combination and the airplane center of gravity. This center-of-pressure location was determined from the expression

$$\frac{x}{\bar{c}} = \frac{C_{m_{W+f}} - C_{m_{Ow+f}}}{C_N}$$

---

<sup>1</sup>The test airplane was not equipped with a hydraulic-boost flow restrictor which limits the maximum rates on most F-86A airplanes to 45° per second.

Over the linear (below the pitch-up) portion of the pitching-moment curves,  $x$  is a constant which coincides with the distance between the wing-fuselage aerodynamic center and the center of gravity, and the two terms may be used interchangeably.

Experimental results.- The variation with Mach number of the zero-lift wing-fuselage pitching-moment coefficient and of the wing-fuselage aerodynamic center for steady level flight is shown in figure 6. The results indicate that the values of  $C_{m_{0w+f}}$ , and, consequently, the balancing tail loads at zero lift, were small and that relatively small variations with Mach number occurred. It should be noted that because of unknown temperature effects on the airplane structure and possibly on the tail strain gages, there is some uncertainty in the values of  $C_{m_{0w+f}}$ , and, consequently, the absolute level of the balancing tail loads. However, the small values of tail load measured at zero lift are reasonable for an airplane having a wing of symmetrical section, indicating that, in the present case, these temperature effects were small. The results in figure 6 also show that a rearward movement of the wing-fuselage aerodynamic center of about 15-percent  $\bar{c}$  occurred as the Mach number was increased from 0.82 to 1.03. At Mach numbers up to about 0.94, the values of aerodynamic center shown in figure 6 are valid only up to the value of  $C_N$  at which the pitch-up occurred. At Mach numbers above 0.96, the aerodynamic-center values shown are valid up to the limit  $C_N$  of the tests. In figure 7, the variation of the wing-fuselage chordwise center of pressure with airplane normal-force coefficient is presented for several values of Mach number. These data show that marked forward, destabilizing shifts in the center of pressure occurred at all Mach numbers up to 0.91. The greatest forward movement occurred at a Mach number of 0.86, approximately the same Mach number at which the pitch-up tendency was most pronounced, according to the pilots. At Mach numbers above about 0.96, no change in the center of pressure occurred over the test  $C_N$  range.

The data in figures 6 and 7, replotted in tail-load form, are presented in figure 8. Shown in this figure are the variation of the total and the aerodynamic balancing tail loads with Mach number for several values of load factor. These data show that, at Mach numbers up to 0.95, the maximum tail loads experienced were fairly small, the total loads generally not exceeding 500 pounds. At Mach numbers above 0.95, however, large down loads were required for balance, the maximum total values exceeding -3200 pounds at a Mach number of about 1.0 and at a load factor of 5. This total load was the maximum recorded during the entire investigation. A time history of a dive and recovery in this critical flight region for balancing tail loads is shown in figure 9.

The foregoing discussion indicates that a critical flight region for balancing tail loads occurred at the highest load factor attained

at a Mach number of 1.03. Figure 10, which presents the tail-load gradients ( $\Delta L_t/\Delta n$ ) for the linear portion of the wing-fuselage pitching-moment curves, shows that this result is a consequence of the large negative shift in the tail-load gradient that was necessary to offset the rearward movement of the wing-fuselage center of pressure at transonic speeds (fig. 6).

Comparison with wind-tunnel data.- An indication of the accuracy with which balancing tail loads may be predicted for design purposes is provided in figure 6 where the wing-fuselage zero-lift pitching-moment coefficient and chordwise center of pressure of additional loading (aerodynamic center) determined from the wind-tunnel data of reference 10 are compared with the flight data for Mach numbers up to 0.90. The wind-tunnel data compare reasonably well with the flight results at zero lift; however, the agreement in center-of-pressure positions is poor. The reason for these discrepancies is not known. Unfortunately, no reliable wind-tunnel data for a model similar in configuration to the test airplane were available to compare with the flight data in the critical region at low supersonic speeds.

Extrapolations.- To provide an indication of the balancing tail loads for design conditions, the flight data were extrapolated to the flight-strength envelope at 35,000 feet and at 12,000 feet.<sup>2</sup> In the pitch-up region where the center of pressure varied with  $C_N$ , the method of extrapolation used was to extend the aerodynamic tail load linearly upward to the flight-strength envelope starting from the point where the center of pressure had reached its most forward position, as indicated by the dashed lines in figure 7. This method of extrapolation was intended to provide a conservative approximation of the balancing loads at the design conditions. The extrapolated balancing tail loads at 35,000 feet and 12,000 feet are shown in figure 11. Results for the test center-of-gravity position of 22.5-percent  $\bar{c}$  show a maximum positive total load of 1700 pounds at a Mach number of 0.65 at 12,000 feet and a maximum negative total load of -5000 pounds at the highest test Mach number of 1.03 at 35,000 feet. At the limiting center-of-gravity positions of 20- and 25-percent  $\bar{c}$ , incremental limit loads of about -1000 and 1000 pounds, respectively, would be obtained. Considering the entire operating range of the airplane as regards Mach number, altitude, and center-of-gravity position, the maximum positive total tail load would be about 2700 pounds and the maximum negative total load would be about -6000 pounds.

---

<sup>2</sup>Lower design altitude for test airplane according to U. S. Air Force specifications.

---

## Maneuvering Tail Loads in Elevator-Pulse Maneuvers

The aerodynamic tail loads discussed in this section are, in general, made up of two parts: One part is proportional to the load factor developed, and the other to the pitching acceleration. Over the range where the aerodynamic derivatives can be considered linear (below the pitch-up), the maneuvering tail-load increment may be written as

$$(\Delta L_{tA})_{\text{man}} = \frac{Wn}{x + l_t} - \frac{I_y}{x + l_t} \ddot{\theta}$$

or

$$(\Delta L_{tA})_{\text{man}} = \left( \frac{\Delta L_{tA}}{\Delta n} \right)_{\text{bal}} n + \left( \frac{\Delta L_t}{\Delta \ddot{\theta}} \right) \ddot{\theta}$$

Experimental results.- A typical time history of the airplane response to an elevator pulse is shown in figure 12. The results in figure 12 show that the first-peak tail-load increment occurred near the maximum down-elevator deflection and before the airplane had responded appreciably in terms of load factor. The second-peak load occurred at about the maximum load-factor increment and just after the elevator had been returned to its trim position. From inspection of the records obtained during the elevator-pulse maneuvers, both the first-peak pitching acceleration and tail load were found to be primarily a linear function of the maximum elevator-deflection increment as shown in figure 13. The variation with Mach number of the first-peak pitching acceleration for a unit increment in maximum elevator deflection is shown in figure 13(a). In figure 13(b), the variation with Mach number of the measured first-peak load for a unit increment in maximum elevator deflection is presented. Also shown in figure 13(b) for comparison with the measured loads are the first-peak values estimated from the simplified relationship.

$$\frac{\Delta L_{tA}}{\Delta \delta_e} = \left( - \frac{I_y}{x + l_t} \right) \frac{\ddot{\theta}}{\Delta \delta_e}$$

which may be used because the load factor had not changed appreciably in the time interval the pitching acceleration built up to the first-peak value. (See fig. 12.) The agreement shown in figure 13 between the loads estimated from the measured pitching accelerations and the measured loads is good. The maximum first-peak tail-load gradients with respect to elevator deflection were experienced at a Mach number of 0.80. At higher Mach numbers they dropped off rapidly until, at low supersonic speeds,

they were only about one-fourth their maximum subsonic values. This decrease corresponds to the rapid loss in elevator effectiveness that occurs on the test airplane at transonic speeds. Figure 14 presents the first-peak data in the form  $\dot{\theta}_1/\Delta n_{\max}$  and  $\Delta L_{tA_1}/\Delta n_{\max}$  for the purpose of a later extrapolation to design conditions. The increased scatter of the data compared with that in figure 13 is mainly attributable to variations in control frequency. The decrease in the maximum values of  $\dot{\theta}_1/\Delta n_{\max}$  and  $\Delta L_{tA_1}/\Delta n_{\max}$  to about one-half their subsonic-speed value at supersonic speeds is due, primarily, to an increase in the airplane frequency and a decrease in control frequency (corresponding to a decrease in frequency ratio  $\omega_1/\omega$  from about 3 to 0.7). This decrease in frequency ratio altered the variation of load-factor response with increasing speed while leaving the first-peak tail-load variation relatively unchanged.

The second-peak pitching acceleration and tail-load increment for a unit increment in load factor are shown in figures 15(a) and 15(b), respectively. The tail-load values indicated by the circle symbols in figure 15(b) were estimated by adding to the balancing tail-load gradient (fig. 10) the tail load necessary to produce the second-peak pitching-acceleration gradient (fig. 15(a)). These values may be compared with the measured second-peak tail-load gradients indicated by the square symbols in figure 15(b). The comparison shown is fairly good. The second-peak load gradient decreased to about one-half its maximum subsonic-speed value at low supersonic speeds. This decrease resulted primarily from the balancing tail-load gradient assuming a large negative value, which more than offset the large increase in second-peak pitching-acceleration gradient at transonic speeds. A factor contributing to the decrease in second-peak tail-load gradient was the decrease in control frequency  $\omega_1$ , as shown in figure 5(c).

Comparison with computed results.- To provide some information on the accuracy with which the maneuvering tail-load increments may be predicted, computations were made by the procedure described in reference 11 to obtain: (1) time histories of load factor, pitching acceleration, and tail-load response to an elevator pulse at a Mach number of 0.59 at 35,000 feet; and (2) variation of first-peak and second-peak tail-load gradients with control frequency  $\omega_1$  over a range of  $\omega_1$  from 0 to 10 radians per second at Mach numbers of 0.59, 0.85, and 1.0 at 35,000 feet. The pertinent aerodynamic derivatives required for the computations were obtained from reference 8.

Comparison between the computed and the flight results for the time history, as shown in figure 16, indicates that the pitching-acceleration and load-factor variations and the first-peak tail load are predicted fairly well, while the computed second-peak tail load is

quite conservative.<sup>3</sup> If the second-peak tail loads were computed for a given maximum load factor, in accordance with normal design practice, the computed second-peak tail loads would be brought into better agreement with the measured loads.

Comparison of computed and experimental values over a range of control frequencies at Mach numbers of 0.59, 0.85, and 1.0 is presented in figure 17. The comparison at a Mach number of 0.59 in figure 17(a) shows that, at the frequencies for which the flight data were obtained, both the first-peak and second-peak load gradients were overestimated by about 200 pounds per unit load factor. In figure 17(b), the comparison at a Mach number of 0.85 indicates that the computed tail loads are somewhat conservative, although the increase in load gradients with increase in control frequency was predicted fairly well by the computed results. The comparison at a Mach number of 1.0 in figure 17(c) shows that the computed results predicted the first-peak tail-load gradients accurately, although they underestimated the second-peak values by about 150 pounds per unit load factor.

Extrapolations.- In order to provide an indication of the total maneuvering tail loads at the design load factors, the flight results were extrapolated to the flight-strength envelopes at 35,000 feet and at 12,000 feet. The method of extrapolation to obtain the total critical loads over the Mach number range was as follows:

For the first-peak loads

$$L_{tT_{man}} = \left[ \left( -\frac{I_y}{x + l_t} \frac{\ddot{\theta}_1}{\Delta n_{max}} + \frac{\ddot{\theta}_1}{\Delta n_{max}} \frac{l_t}{g} W_t \right) (n_{des} - 1) + L_{tT_{bal}(n=1.0)} \right]$$

where values of  $n_{des}$  were obtained from the design load-factor boundaries in figure 4; values of  $\ddot{\theta}_1/\Delta n_{max}$  were obtained from figure 14; and values of  $L_{tT_{bal}(n=1.0)}$  were obtained from figure 8.

For the second-peak loads

$$L_{tT_{man}} = \left[ \left( -\frac{I_y}{x + l_t} \frac{\ddot{\theta}_2}{\Delta n_{max}} + \frac{\ddot{\theta}_2}{\Delta n_{max}} \frac{l_t}{g} W_t \right) (n_{des} - 1) + L_{tT_{bal}(n=n_{des})} \right]$$

---

<sup>3</sup>The effect of a difference in the assumed and the experimental elevator inputs was checked on a Reeves Analogue Computer and found to be negligible.

---

where the  $\ddot{\theta}_z/\Delta n_{\max}$  values were obtained from figure 15 and values of  $L_{Tbal}(n=n_{des})$  were obtained from figure 11. The first-peak total loads, extrapolated in this manner are presented in figure 18. The values in figure 18(a) at 35,000 feet indicate that a critical first-peak load of about -6000 pounds would be experienced at about 0.85 Mach number. At lower Mach numbers, the loads decreased rapidly due to the decrease in load factor at the flight-strength envelope. At higher Mach numbers, a rapid decrease in load also occurred, apparently the effect of the assumed decrease in frequency ratio  $\omega_1/\omega$ .<sup>4</sup> At 12,000 feet the critical first-peak load of about -7800 pounds would be experienced at relatively low Mach number as shown in figure 18(b). The loads drop off rapidly at transonic speeds again, due primarily to the effect of the assumed decrease in frequency ratio  $\omega_1/\omega$ .

The extrapolated second-peak total loads are presented in figure 19. As shown by the data in figure 19(a), a critical load at 35,000 feet of about 4900 pounds would be experienced at a Mach number of about 0.90. Above a Mach number of 0.90, the loads decrease rapidly, primarily as the result of the negative shift in the balancing-load gradient at transonic speeds. The effect of a decrease in control frequency above a Mach number of 0.93 also contributes to the decrease in second-peak loads at transonic speeds. The results in figure 19(b) for 12,000 feet indicate that a critical load of about 5000 pounds would be experienced at the lowest test Mach number of about 0.60. The decrease in the second-peak loads that occurs at transonic speeds again may be shown to result from a large negative change in the balancing tail-load gradient and a reduction in control frequency.

In the extrapolations shown in figures 18 and 19, it was assumed that the test airplane would have sufficient control power to reach the design load factors at all test Mach numbers at 35,000 feet and 12,000 feet, using the measured control frequencies. Actually, this is not the case for this airplane and the results shown are therefore somewhat conservative.

#### Maneuvering Tail Loads in Pitch-Up Maneuvers

Pitch-ups of the test airplane due to a decrease in wing-fuselage stability with an increase in normal-force coefficient at constant Mach number and due to a decrease in wing-fuselage stability with a decrease in Mach number at constant normal-force coefficient were sources of relatively large maneuvering loads on the horizontal tail. Time histories

---

<sup>4</sup>For these extrapolations, the elevator-control frequencies at the design load factors were assumed the same as the measured values shown in figure 5(c).

---

of two pitch-ups resulting from variations of normal-force coefficient<sup>5</sup> and Mach number<sup>6</sup> are shown in figures 20 and 21, respectively. The large positive aerodynamic loads experienced during these maneuvers arose when the pilot, abruptly applying corrective control to arrest the pitch-up, introduced positive maneuvering tail-load increments which reinforced the normal positive increase in the balancing loads in these flight regions. (See fig. 8.) A peak aerodynamic tail load of about 2200 pounds is shown in figure 20. Although no pitching-velocity records were available for this maneuver, analysis of other available records shows that maximum positive and negative pitching accelerations of 0.6 and -1.8 radians per second per second were experienced, which corresponds to tail loads of about -600 pounds and 1700 pounds, respectively. A somewhat lower peak aerodynamic tail load of 1500 pounds is indicated in figure 21. The maximum pitching accelerations recorded in this pitch-up maneuver were 0.44 and -0.72 radians per second per second corresponding to tail loads of about -400 and 700 pounds, respectively.

These pitch-up maneuvers were recorded by experienced pilots whose reaction and application of corrective control may not have been as abrupt and violent as would be those of a pilot experiencing the pitch-up for the first time. Also, even experienced pilots may, under certain circumstances, apply excessive corrective control abruptly, thereby introducing large maneuvering load increments on the horizontal tail at high load factor. It appears then that this type of maneuver is a realistic approximation to the Air Force design pull-up push-down maneuver and is appropriate for predicting design maneuvering tail loads for swept-wing airplanes.

#### Buffet Tail Loads

The total buffet tail-load increments measured in these tests, which extended beyond the buffet boundary as indicated by the circle symbols in figure 4, were evaluated from records of the type shown in figure 22. The peak actuator and clevis-bolt buffet loads (fig. 22) occurred at about the same time instant, so that with little error the buffet-load increment could be given as

$$\Delta L_{TT} = \pm \left( \frac{\Delta F_A + \Delta F_{C.B.}}{2} \right)$$

---

<sup>5</sup>The Mach number is essentially constant up to the onset of the pitch-up, after which it may decrease rapidly due to the rapid increase in drag. (See fig. 20.)

<sup>6</sup>As the Mach number decreases through about 0.95 (fig. 21), a pitch-up occurs due to an abrupt decrease in wing-fuselage stability at the higher values of  $C_N$ . (See ref. 8.)

---

where  $\Delta F_A$  and  $\Delta F_{C.B.}$  are the algebraic peak-to-valley changes in the actuator and clevis-bolt loads, respectively. The maximum buffet tail-load increments are presented in figure 23. It is recognized that these results do not necessarily represent the maximum buffet tail-load increments attainable for the flight regions investigated because statistical studies (ref. 12) indicate that the peak wing buffet loads increase the longer the airplane is flown in a given flight region. However, in view of the large number of test runs from which these results were drawn, it is felt the values shown in figure 23 would not be appreciably increased if additional data were obtained. The results show relatively small total buffet-load increments over the entire Mach number load-factor range tested, the loads varying from about  $\pm 500$  pounds at Mach numbers up to 0.85 to nearly zero at low supersonic Mach numbers. The predominant frequency of these incremental buffeting loads was about 12 cycles per second, corresponding to the lowest vertical bending frequency of the fuselage. It should be pointed out that though the buffet loads were relatively low, a fatigue crack in the stabilizer rear-spar carry-over plate was noted after about 100 flying hours, 2 of which were flown in the buffeting region.

A comparison of the maximum incremental buffet tail-load coefficients for the swept-wing test airplane with those for a straight-wing airplane is shown in figure 24. The values for the latter were obtained from reference 13. The straight-wing airplane had wing and tail thickness ratios of about 14 and 11 percent, respectively, as compared with values in the streamwise direction of about 9 and 8 percent, respectively, for the swept-wing test airplane. Over a comparable Mach number range, the maximum buffet tail-load increments for the swept-wing test airplane were only about 30 percent of those for the straight-wing airplane.

A comparison between buffet tail-load coefficients obtained experimentally and by estimation using the procedure outlined in reference 14 is shown in figure 25. The estimated values are highly conservative.

#### Tail-Load Distributions

The results given in figures 26 to 29 show the distribution of over-all horizontal-tail loads between the stabilizer actuator and the two clevis bolts for several flight conditions. The actuator and clevis-bolt loads presented herein are normal (perpendicular to the plane containing the airplane longitudinal and lateral axes) loads. Chordwise center-of-pressure data for the loadings shown in figures 26 to 29 are presented in figure 30.

The support loads in the critical flight region for balancing tail loads are shown in figure 26. An extrapolation of these results to the design load factor of 7.33 indicates a load of about -9300 pounds on the

two clevis bolts and 4500 pounds on the actuator. Figure 27 presents the horizontal-tail support loads for the severe pitch-up at constant Mach number shown previously in figure 20. The buffet-load increments are also indicated in figure 27 by the shaded areas. Maximum support loads (including the buffet-load increments) of about 7200 pounds and -5700 pounds are indicated for the two clevis bolts and the horizontal-tail actuator, respectively. The horizontal-tail support loads for a unit increment in load factor are given in figure 28 for the elevator-pulse maneuvers. Maximum first-peak support loads of about -3500 pounds on the two clevis bolts and 2700 pounds on the actuator for a unit increment in load factor are shown in figure 28(a). Maximum second-peak loads on the clevis bolts and actuator of 1800 pounds and -1650 pounds, respectively, for a unit increment in load factor are indicated in figure 28(b). The maximum buffet-load increments on the horizontal-tail supports (fig. 29) reached a maximum of about  $\pm 2400$  pounds at a Mach number of 0.83. At higher Mach numbers, the buffet loads decreased rapidly, approaching zero at low supersonic speeds.

The chordwise centers of pressure of the horizontal tail based on the experimental results (fig. 30)<sup>7</sup> ranged from about 20 percent of the mean aerodynamic chord for the second-peak-load increments in the elevator-pulse maneuvers ( $\Delta S_e \approx 0$ ) to about 90 percent of the mean aerodynamic chord for the first-peak-load increments in the pulse maneuvers ( $\Delta \alpha_t \approx 0$ ). The center of pressure for the maximum load recorded in a severe pitch-up (figs. 20 and 27) was located at about 48 percent of the tail mean aerodynamic chord. For the critical balancing load, the center of pressure was located at about 47 percent of the mean aerodynamic chord.

### CONCLUSIONS

Flight tests conducted on a swept-wing fighter airplane over a Mach number range of 0.60 to about 1.03 at 35,000 feet have indicated critical flight regions for balancing, maneuvering, and buffeting tail loads. From the test results and their analysis the following conclusions were drawn:

1. Extrapolation of the test results to the design limits indicated maximum balancing total tail loads of 1700 pounds and -5000 pounds. The -5000-pound load occurred at the highest test Mach number of 1.03 as a result of a rearward movement of the wing-fuselage center of pressure with increasing Mach number.

---

<sup>7</sup>The chordwise center-of-pressure data at Mach numbers above about 0.92 are not presented for the elevator-pulse maneuvers because of the small loads developed and, consequently, the increasing importance of the tail drag and weight moments, which were neglected in the present analysis.

---

2. Both the extrapolated first-peak and second-peak maneuvering loads in elevator-pulse maneuvers were found to attain critical total values, -8000 pounds and 5000 pounds, respectively, over the design range, at Mach numbers less than 0.90. At high Mach numbers, reduced control effectiveness, negative balancing tail loads, and reduced elevator-control frequencies attained in the flight tests, all conspired to produce lower maneuvering loads.

3. Abrupt stability changes with changing load factor or varying Mach number caused pitch-ups which the pilot checked by rapid control motions. The resulting maneuver was considered a realistic approximation to the pull-up push-down maneuver specified by Air Force load specifications and resulted in relatively high positive tail loads.

4. The maximum buffet tail loads experienced during the investigation were only about  $\pm 500$  pounds, even though the tests covered load factors twice those of the buffet boundary. The maximum loads were experienced at Mach numbers less than 0.85.

5. For loading due primarily to angle of attack, the center of pressure on the tail was in the vicinity of  $0.25 \bar{c}_t$  for Mach numbers up to 0.92, the highest for which data were available. For loading due primarily to elevator deflection, the center of pressure varied from about  $0.5 \bar{c}_t$  at a Mach number of 0.6 to  $0.9 \bar{c}_t$  at a Mach number of 0.91.

6. Comparison between flight results and wind-tunnel data to a Mach number of 0.90 indicated fairly good agreement in the values of  $C_{m_{ow+f}}$ , and, consequently, the balancing tail loads at zero lift; however, poor agreement was obtained between the flight and wind-tunnel values of the wing-fuselage center of pressure of additional loading (proportional to tail-load gradient with respect to load factor). The first-peak maneuvering tail loads computed from flight and wind-tunnel data agreed closely with experimental loads, while the computed second-peak loads were generally conservative over the Mach number range.

Ames Aeronautical Laboratory  
National Advisory Committee for Aeronautics  
Moffett Field, Calif., July 10, 1953

#### REFERENCES

1. Sadoff, Melvin, Turner, William N., and Clousing, Lawrence A.: Measurements of the Pressure Distribution on the Horizontal-Tail Surface of a Typical Propeller-Driven Pursuit Airplane in Flight. I - Effects of Compressibility in Steady Straight and Accelerated Flight. NACA TN 1144, 1947.

~~CONFIDENTIAL~~

2. Sadoff, Melvin, and Clousing, Lawrence A.: Measurements of the Pressure Distribution on the Horizontal-Tail Surface of a Typical Propeller-Driven Pursuit Airplane in Flight. II - The Effect of Angle of Sideslip and Propeller Operation. NACA TN 1202, 1947.
3. Sadoff, Melvin, and Clousing, Lawrence A.: Measurements of the Pressure Distribution on the Horizontal-Tail Surface of a Typical Propeller-Driven Pursuit Airplane in Flight. III - Tail Loads in Abrupt Pull-Up Push-Down Maneuvers. NACA TN 1539, 1948.
4. Garvin, John B.: Flight Measurements of Aerodynamic Loads on the Horizontal Tail Surface of a Fighter-Type Airplane. NACA TN 1483, 1947.
5. Mayer, John P., Valentine, George M., and Mayer, Geraldine C.: Flight Measurements with the Douglas D-558-II (BuAer No. 37974) Research Airplane. Determination of the Aerodynamic Center and Zero-Lift Pitching-Moment Coefficient of the Wing-Fuselage Combination by Means of Tail-Load Measurements in the Mach Number Range from 0.37 to 0.87. NACA RM L50D10, 1950.
6. Rogers, John T., and Dunn, Angel H.: Preliminary Results of Horizontal Tail-Load Measurements of the Bell X-5 Research Airplane. NACA RM L52G14, 1952.
7. Triplett, William C., and Van Dyke, Rudolph D., Jr.: Preliminary Flight Investigation of the Dynamic Longitudinal-Stability Characteristics of a 35° Swept-Wing Airplane. NACA RM A50J09a, 1950.
8. Anderson, Seth B., and Bray, Richard S.: A Flight Evaluation of the Longitudinal Stability Characteristics Associated with the Pitch-Up of a Swept-Wing Airplane in Maneuvering Flight at Transonic Speeds. NACA RM A51I12, 1951.
9. Thompson, Jim Rogers, Bray, Richard S., and Cooper, George E.: Flight Calibration of Four Airspeed Systems on a Swept-Wing Airplane at Mach Numbers up to 1.04 by the NACA Radar-Phototheodolite Method. NACA RM A50H24, 1950.
10. Morrill, Charles P., Jr., and Boddy, Lee E.: High-Speed Stability and Control Characteristics of a Fighter Airplane Model with a Swept-Back Wing and Tail. NACA RM A7K28, 1948.
11. Sadoff, Melvin: On the Use of a Damped Sine-Wave Elevator Motion for Computing the Design Maneuvering Horizontal-Tail Load. NACA TN 2877, 1953.

12. Liepmann, H. W.: On the Application of Statistical Concepts to the Buffeting Problem. Jour. Aero. Sci., vol. 19, no. 12, Dec. 1952.
13. Stokke, Allen R., and Aiken, William S., Jr.: Flight Measurements of Buffeting Tail Loads. NACA TN 1719, 1948.
14. Bouton, Innes, and Madrick, A. H.: Structural Criterion for Buffeting Tail Loads. McDonnell Aircraft Corp. Rep. 1958, 27 March 1951.

TABLE I.- PHYSICAL CHARACTERISTICS OF TEST AIRPLANE

Wing	
Total wing area (including flaps, slats and 49.92 sq ft covered by fuselage), sq ft . . . . .	287.9
Span, ft . . . . .	37.1
Aspect ratio . . . . .	4.79
Taper ratio . . . . .	0.51
Mean aerodynamic chord (wing station 98.7 in.), ft . . . . .	8.08
Dihedral angle, deg . . . . .	3.0
Sweepback of 0.25-chord line, deg . . . . .	34.23
Aerodynamic and geometric twist, deg . . . . .	2.0
Root airfoil section (normal to 0.25-chord line) . . . . .	NACA 0012-64 (modified)
Tip airfoil section (normal to 0.25-chord line). . . . .	NACA 0011-64 (modified)
Leading-edge slats (each side)	
Total area (projected into wing reference plane), sq ft . . . . .	17.72
Span, ft . . . . .	12.95
Chord (constant), ft . . . . .	1.37
Horizontal tail	
Total area (including 1.20 sq ft covered by vertical tail), sq ft . . . . .	35.0
Exposed area, sq ft . . . . .	30.3
Span, ft . . . . .	12.8
Aspect ratio . . . . .	4.65
Taper ratio . . . . .	0.45
Dihedral angle, deg . . . . .	10.0
Root chord (horizontal-tail station 0), ft . . . . .	3.79
Tip chord (equivalent horizontal-tail station 76.68 in.), ft . . . . .	1.74
Mean aerodynamic chord (horizontal-tail station 33.54 in.) ft . . . . .	2.89
Sweepback of 0.25-chord line, deg . . . . .	34.58
Horizontal-tail length, ft . . . . .	18.25
Airfoil section (parallel to center line). . . . .	NACA 0010-64
Maximum stabilizer deflection, deg . . . . .	1 nose up, 10 nose down
Elevator	
Area (including tabs and excluding balance area forward of hinge line), sq ft . . . . .	10.1
Span (each), ft . . . . .	5.8
Chord, inboard (equivalent horizontal-tail station 6.92 in.), ft . . . . .	1.19
Chord, outboard (theoretical, horizontal-tail station 76.18 in.), ft . . . . .	0.58
Maximum elevator deflection, deg . . . . .	35 up, 17.5 down
Boost . . . . .	hydraulic
Horizontal-tail weight, lb . . . . .	175

~~CONFIDENTIAL~~

NACA RM A53G10

~~CONFIDENTIAL~~

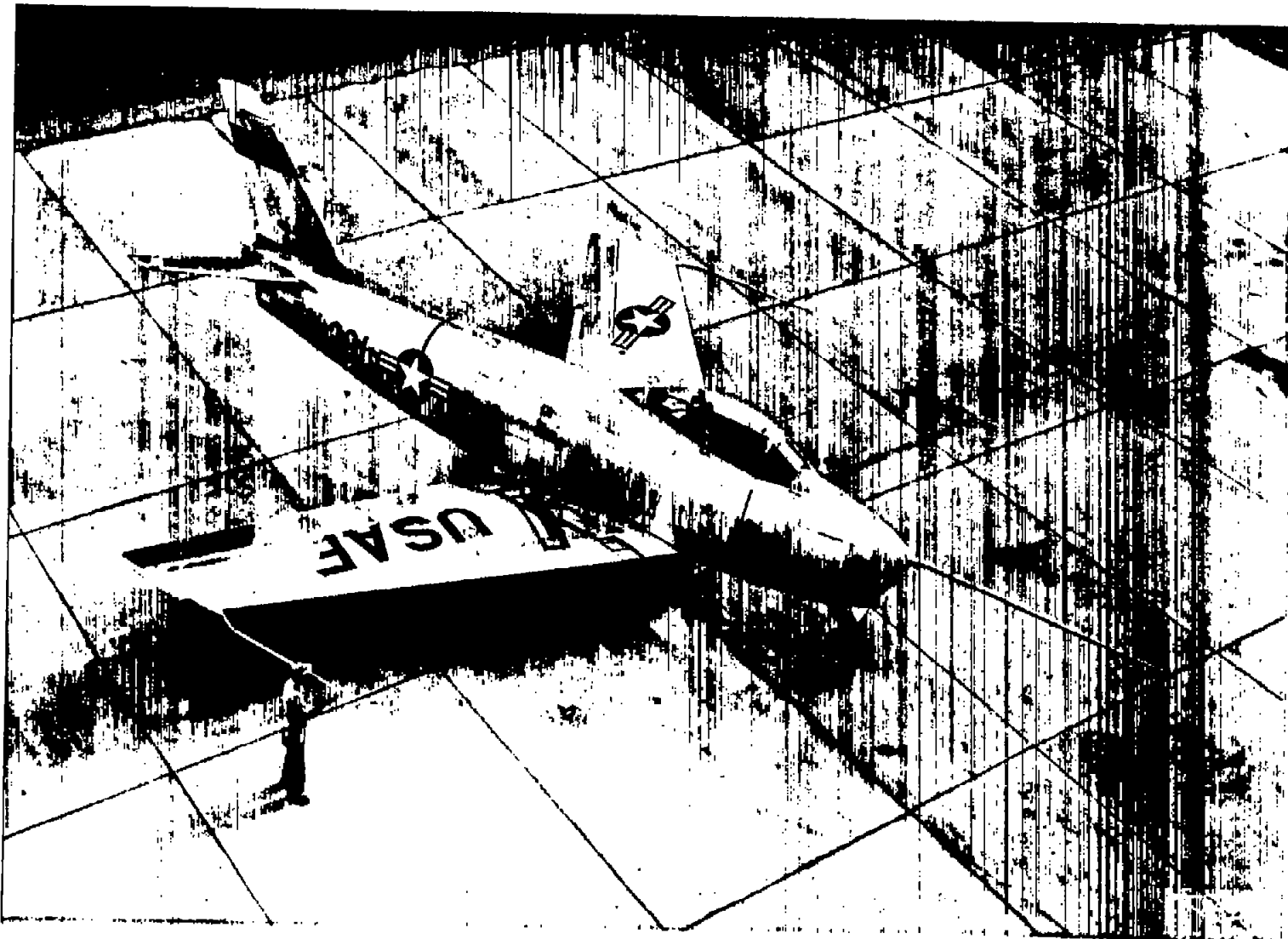


Figure 1.- Photograph of the test airplane.

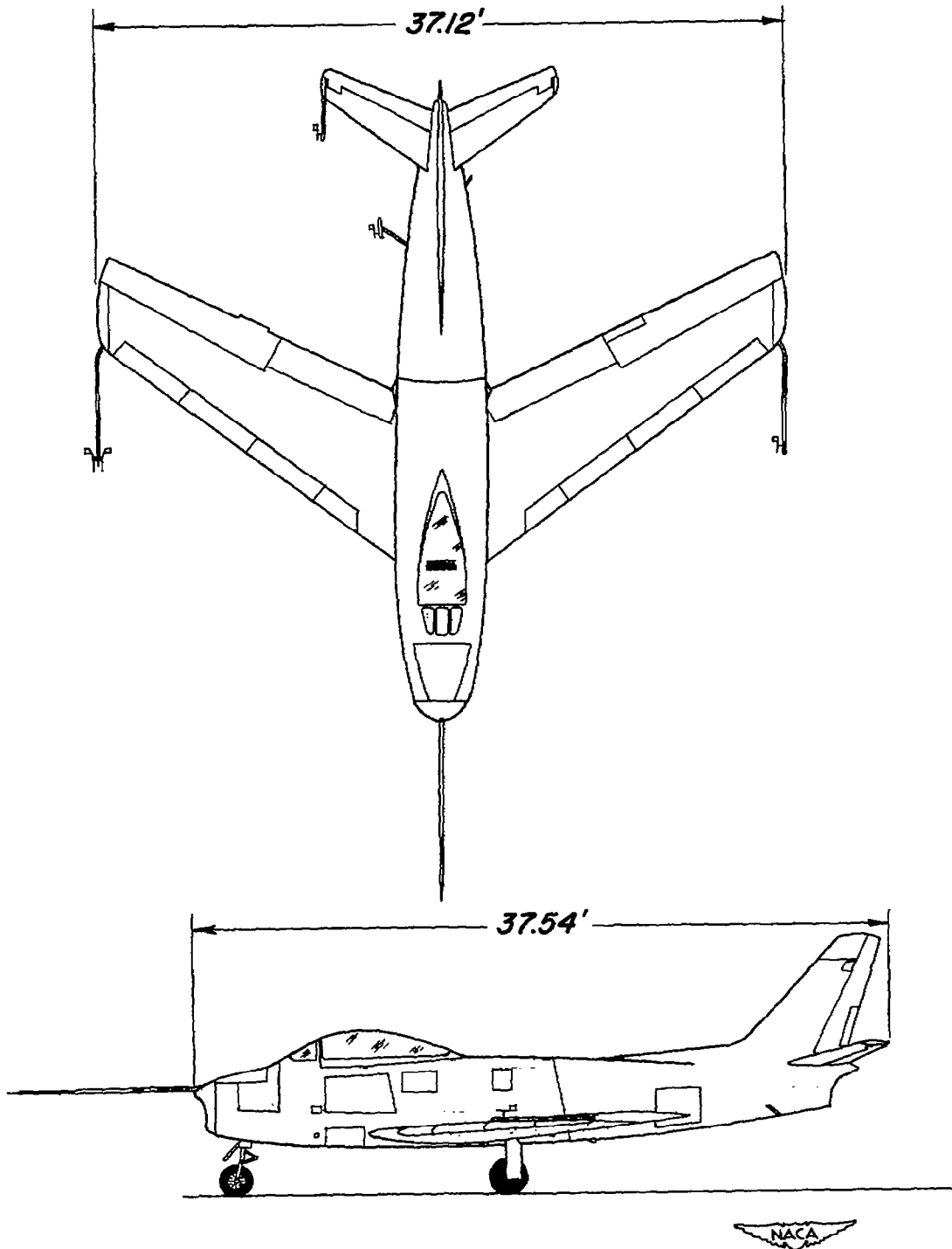


Figure 2.- Two-view drawing of the test airplane.

Note: All dimensions in inches.

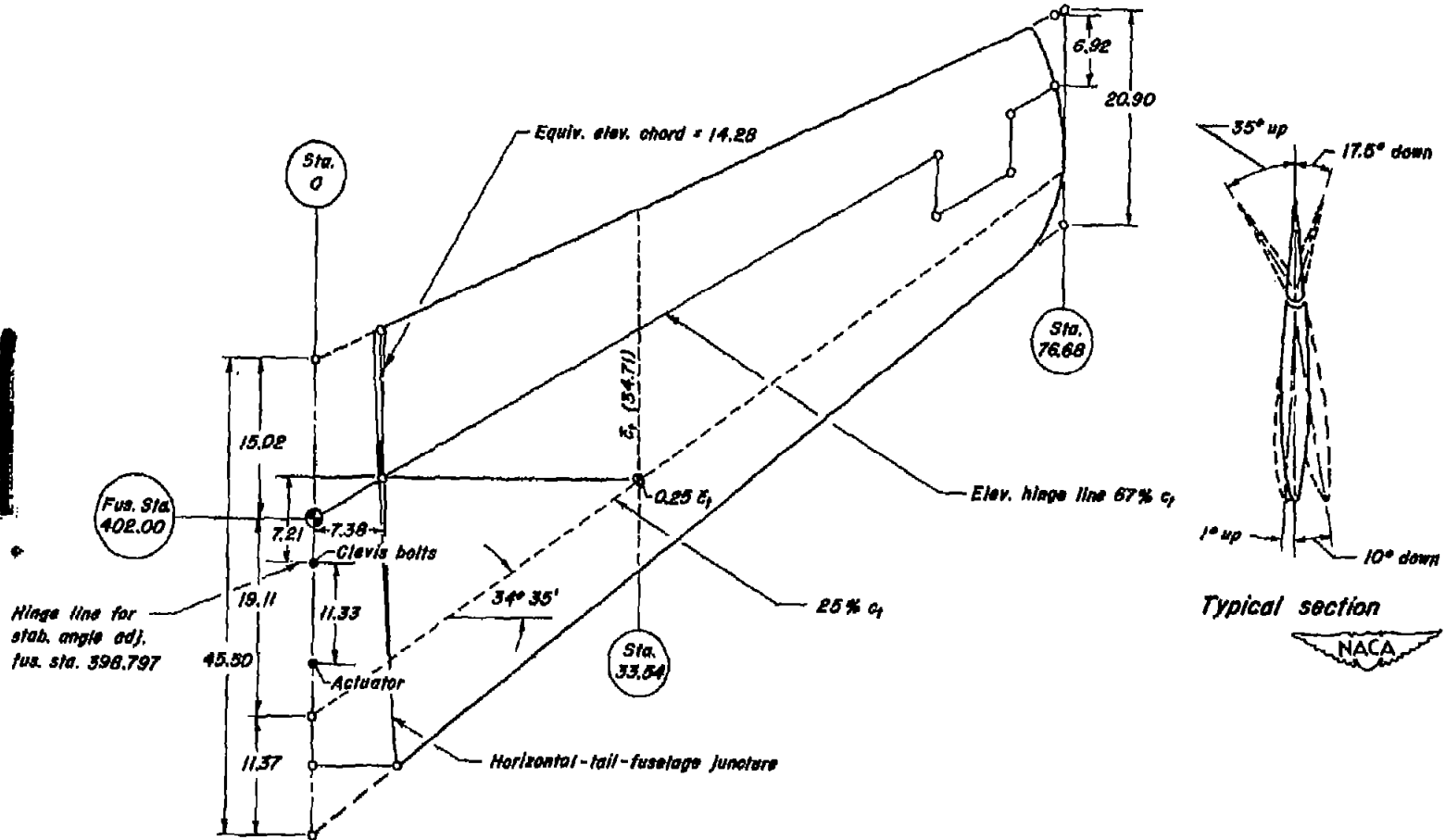
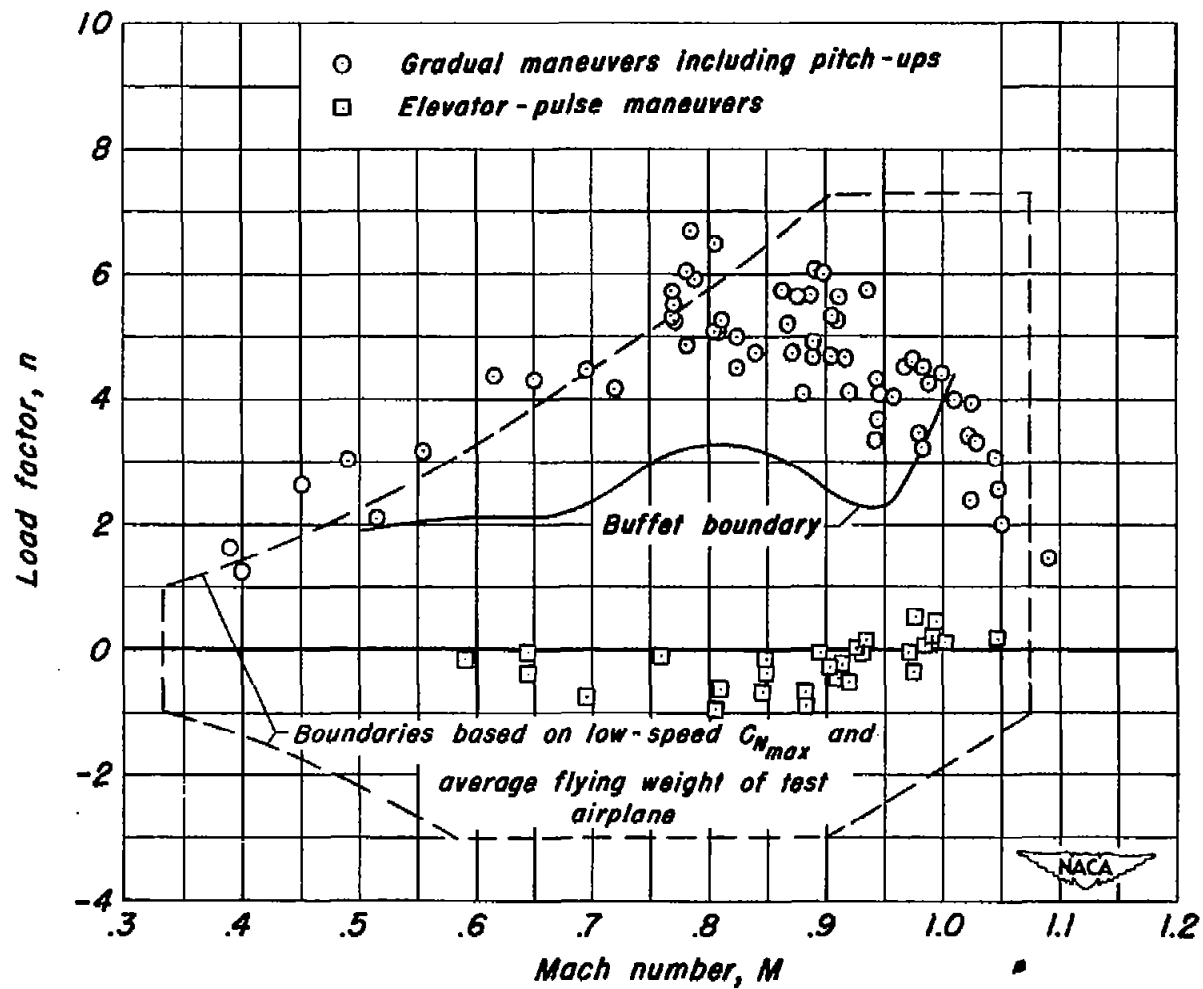
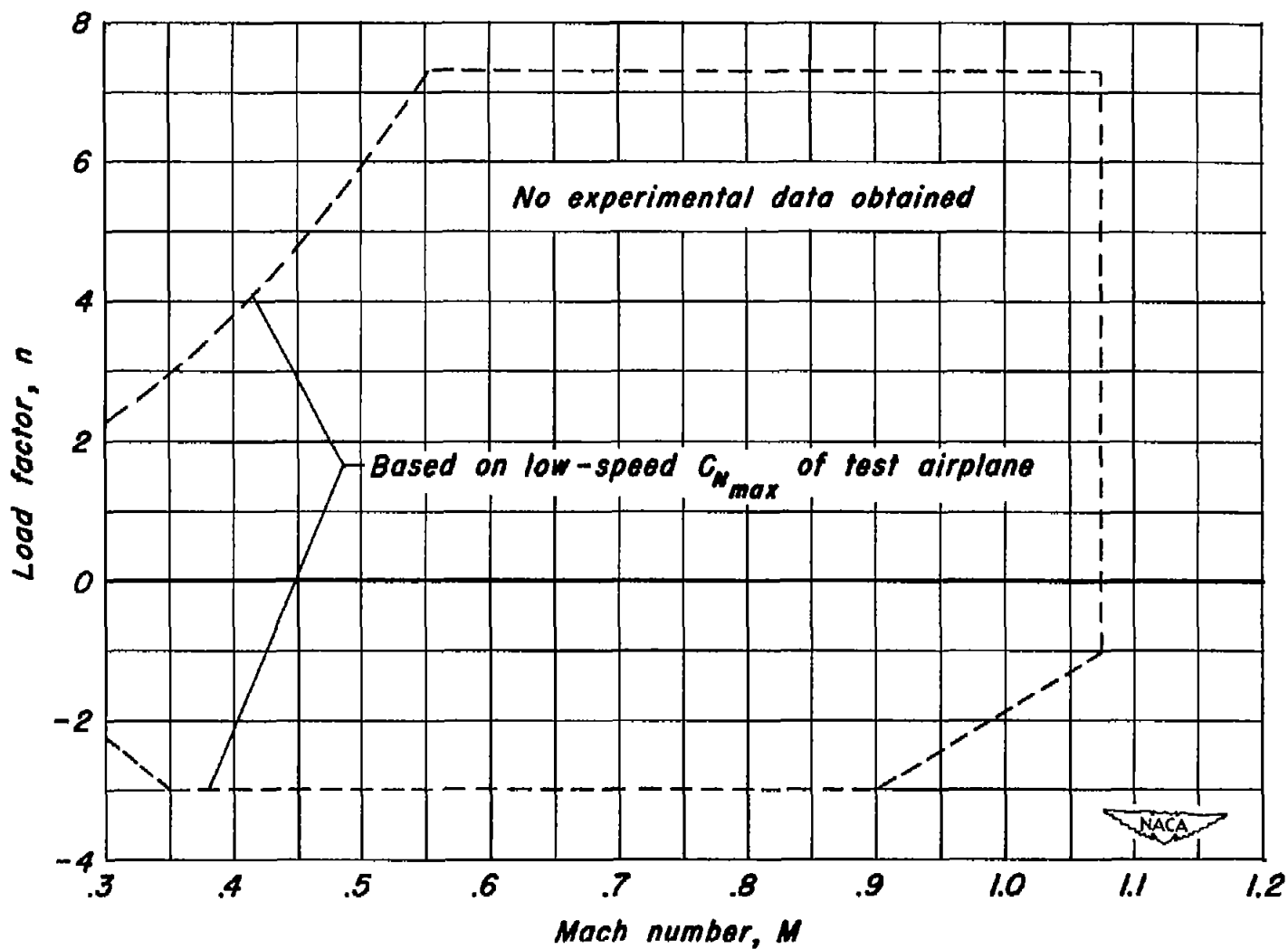


Figure 3.- Geometric characteristics of horizontal tail of test airplane.



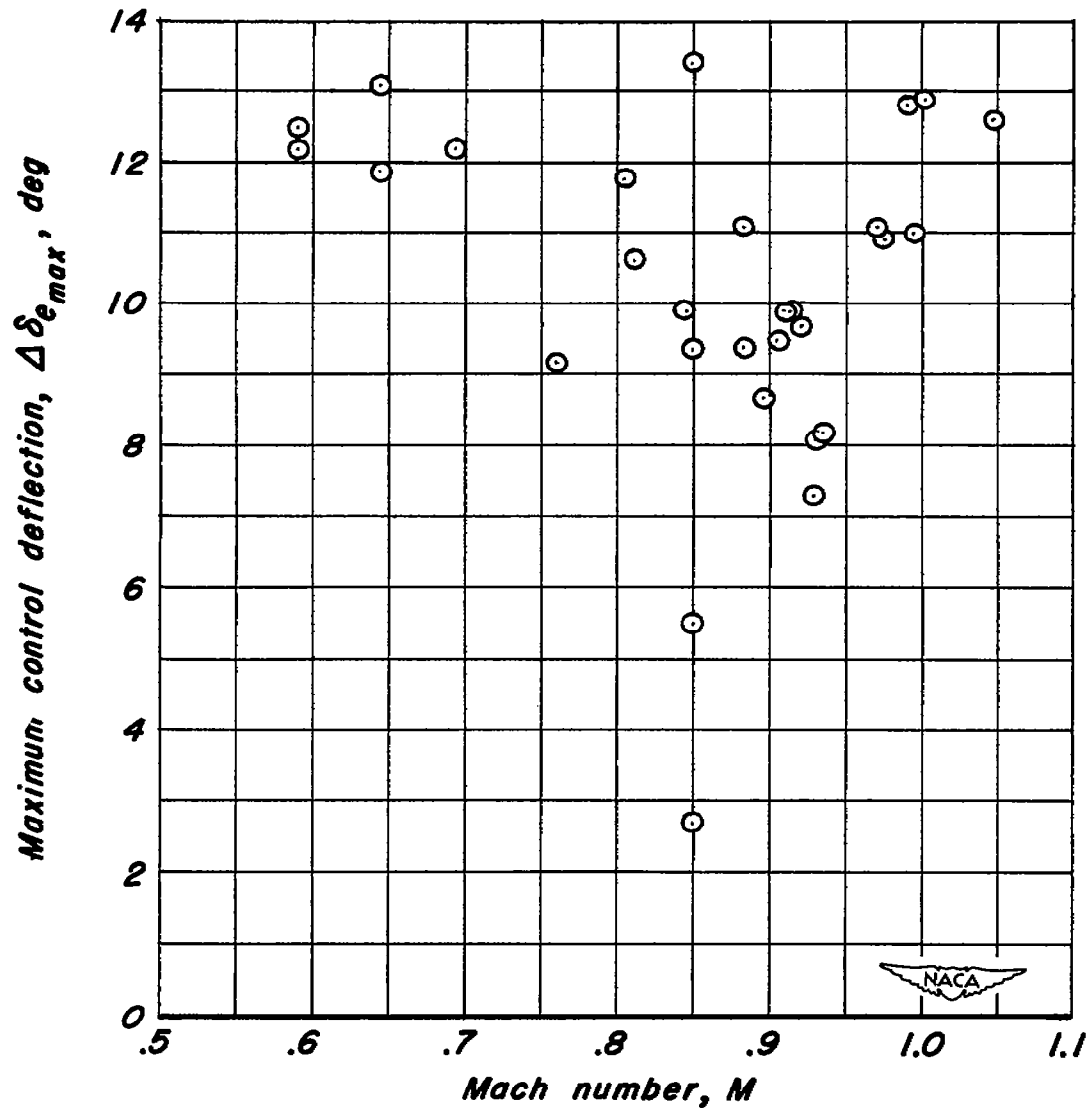
(a) 35,000 feet altitude.

Figure 4.- Flight regions investigated with test airplane.



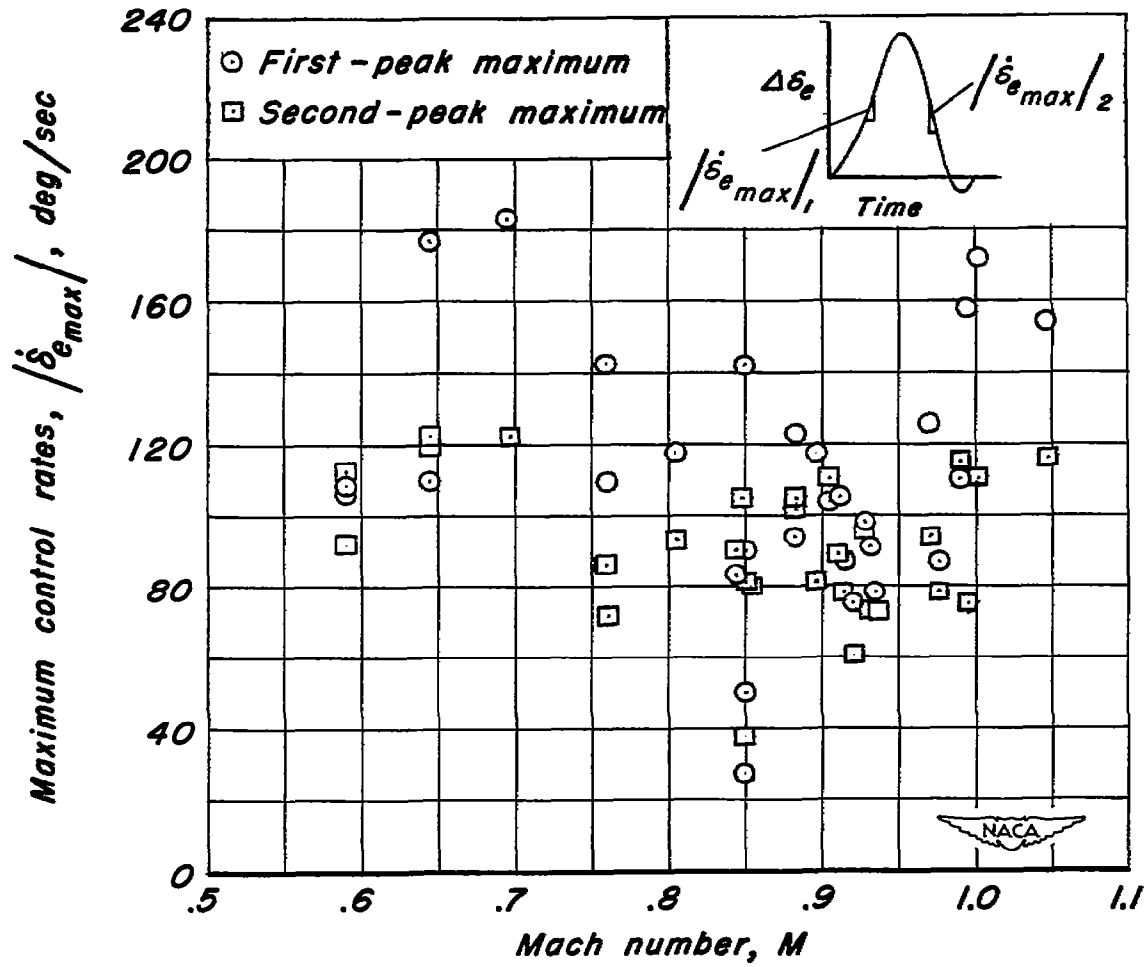
(b) 12,000 feet altitude.

Figure 4.- Concluded.



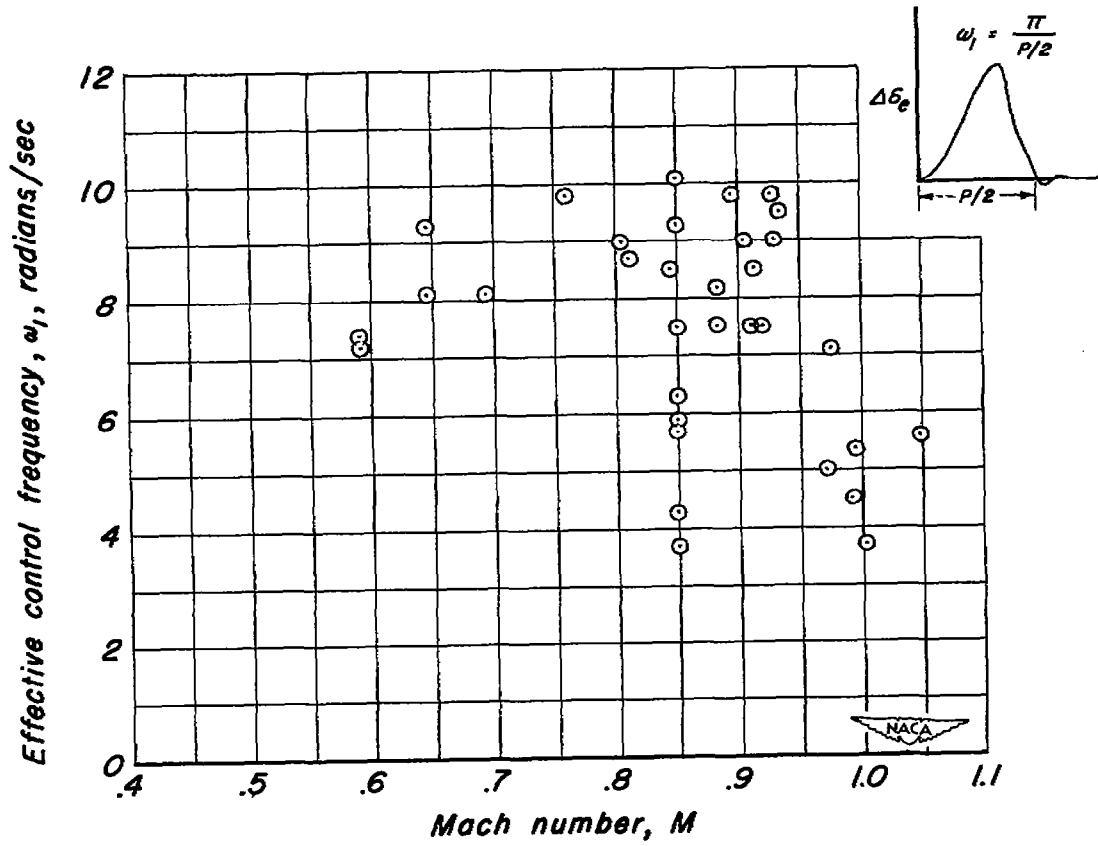
(a) Control deflections.

Figure 5.- Maximum control deflections, control rates and effective control frequencies used in the elevator-pulse maneuvers.



(b) Control rates.

Figure 5.- Continued.



(c) Control frequencies.

Figure 5.- Concluded.

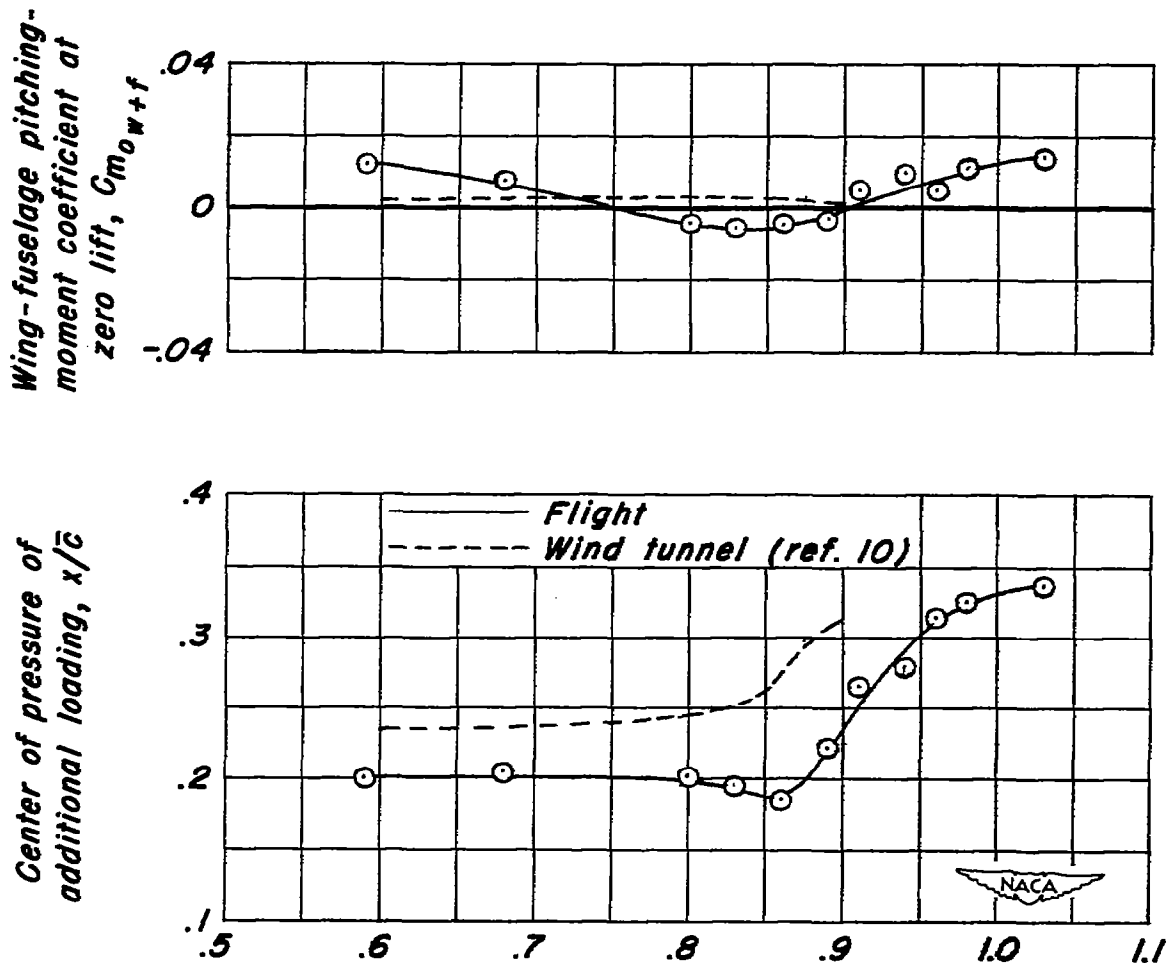


Figure 6.- Variation with Mach number of the wing-fuselage pitching-moment coefficient at zero lift and of the wing-fuselage center of pressure for normal-force coefficients to the pitch-up.

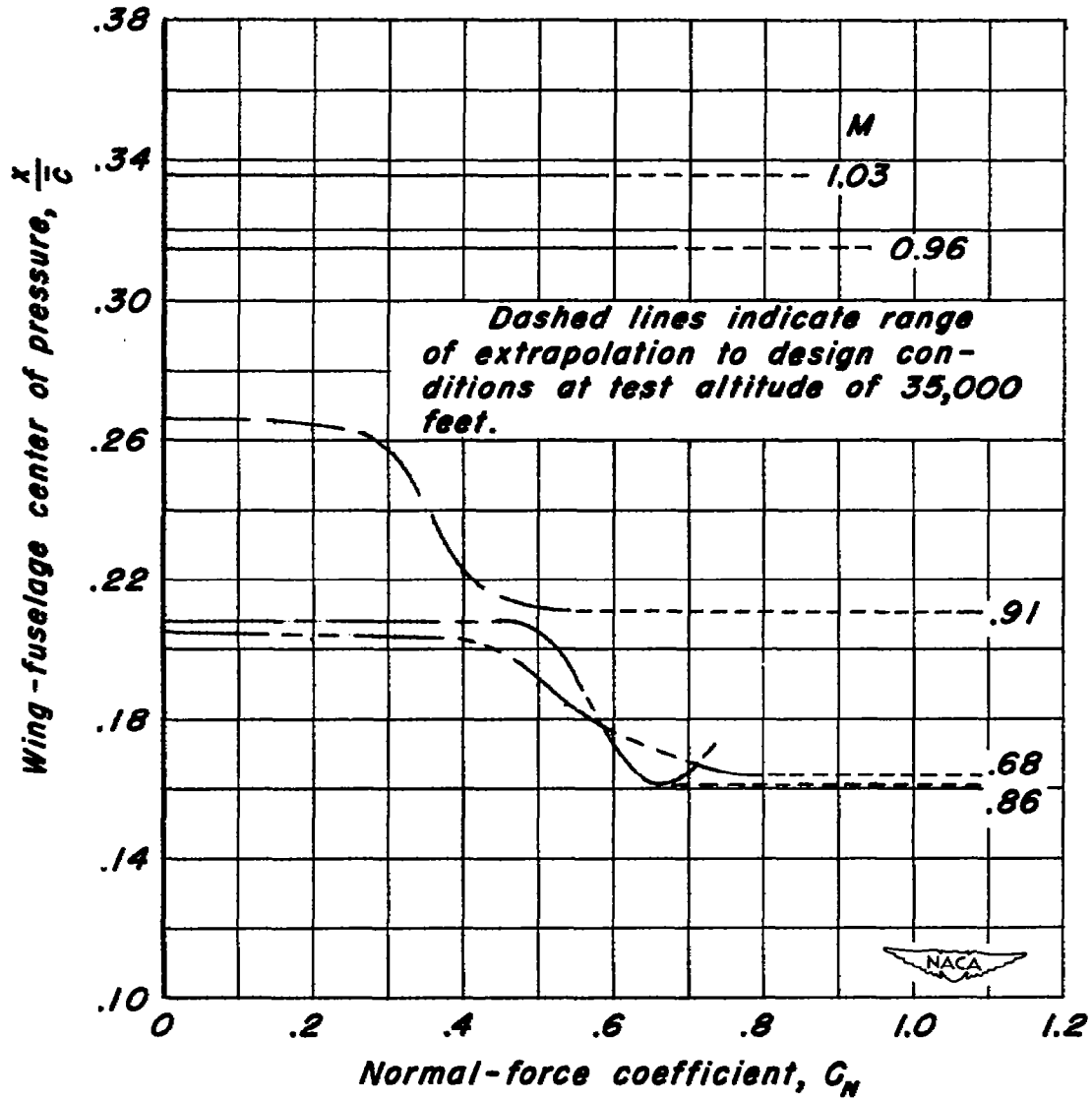


Figure 7.- Variation of the wing-fuselage center of pressure with airplane normal-force coefficient for several values of Mach number.

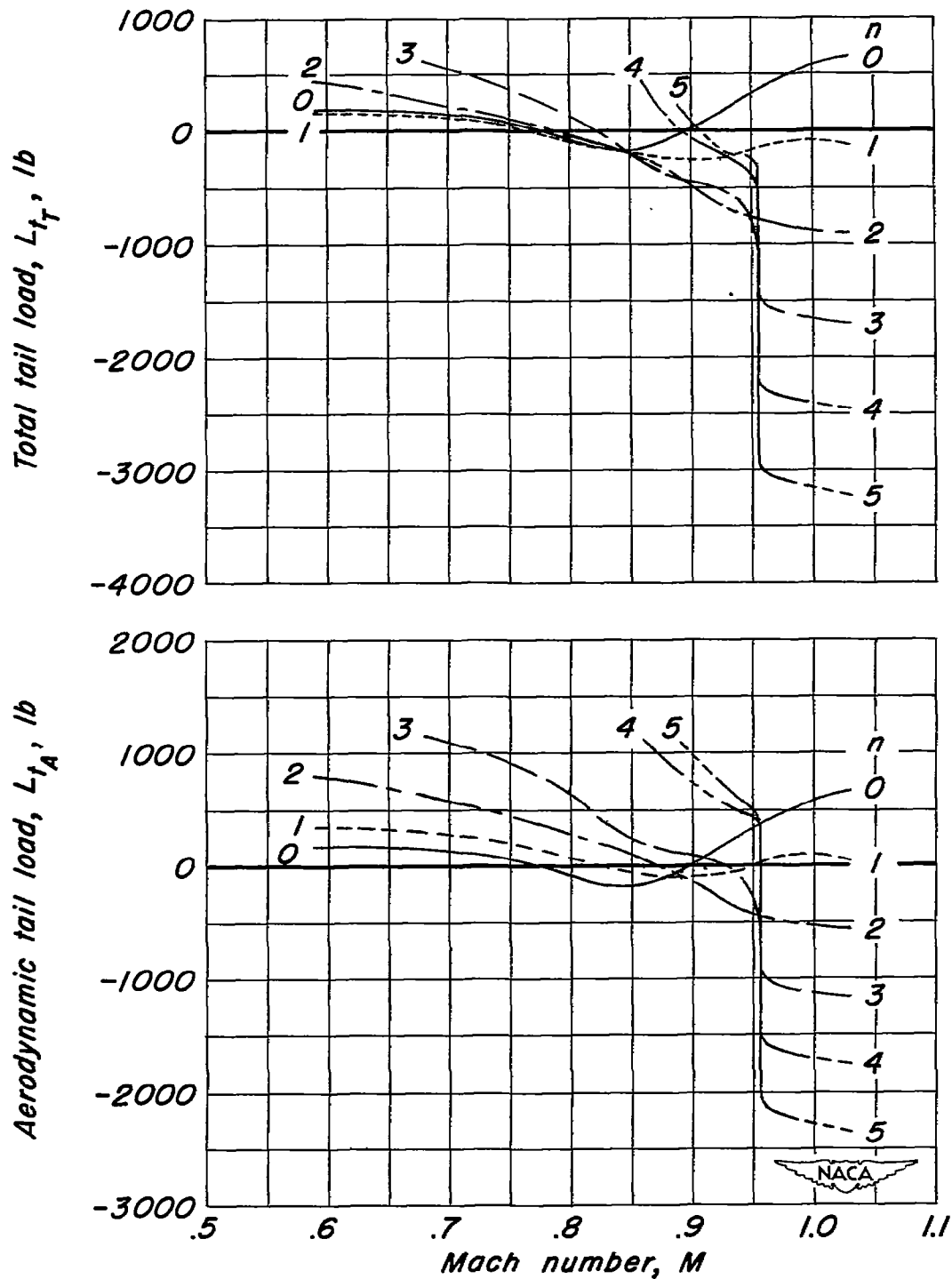


Figure 8.- Variation of the total and the aerodynamic balancing tail load with Mach number for several values of load factor. Pressure altitude, 35,000 feet. Center of gravity, 22.5-percent  $\bar{c}$ .

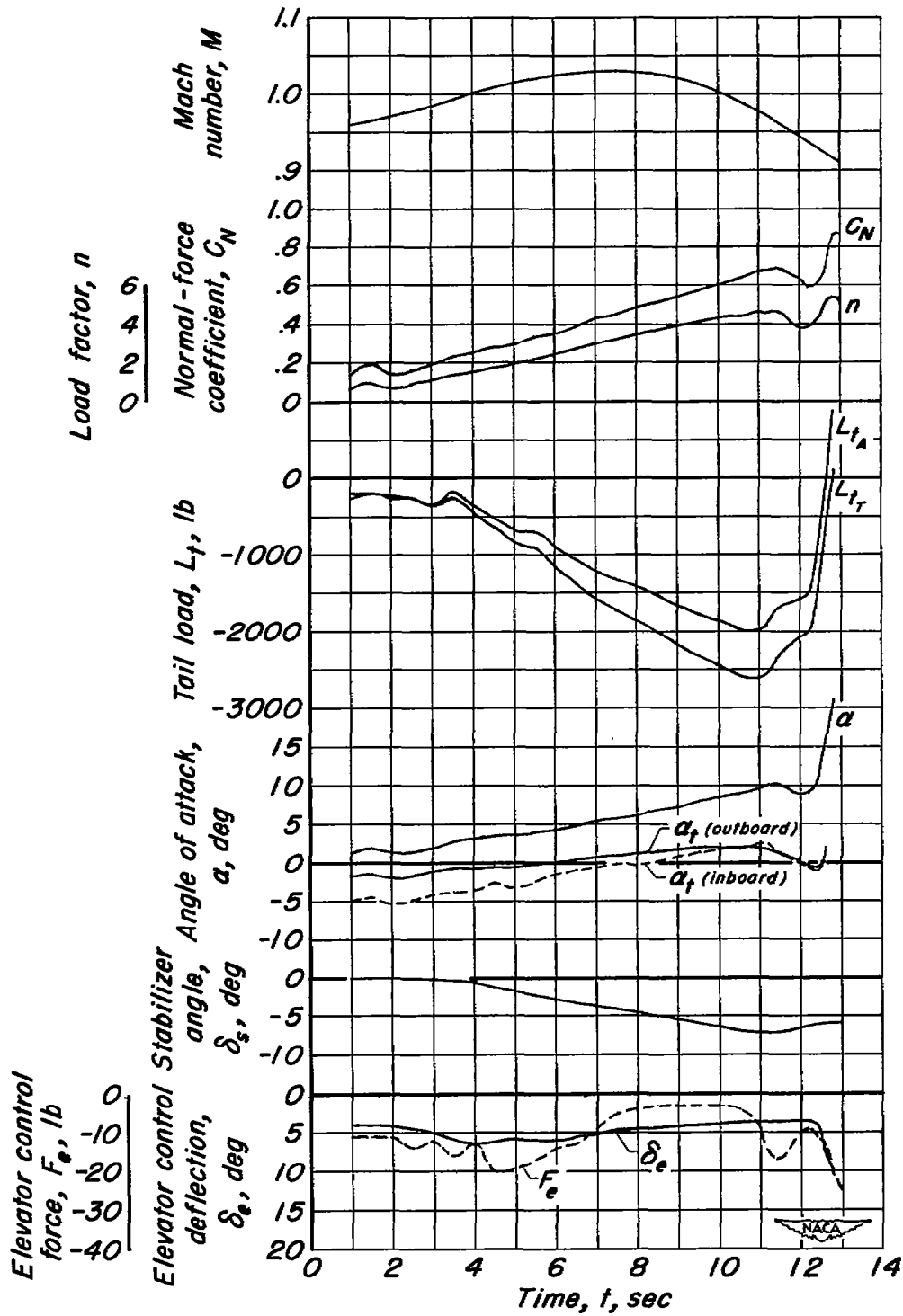


Figure 9.- Time history of a dive and pull-out at transonic speed.

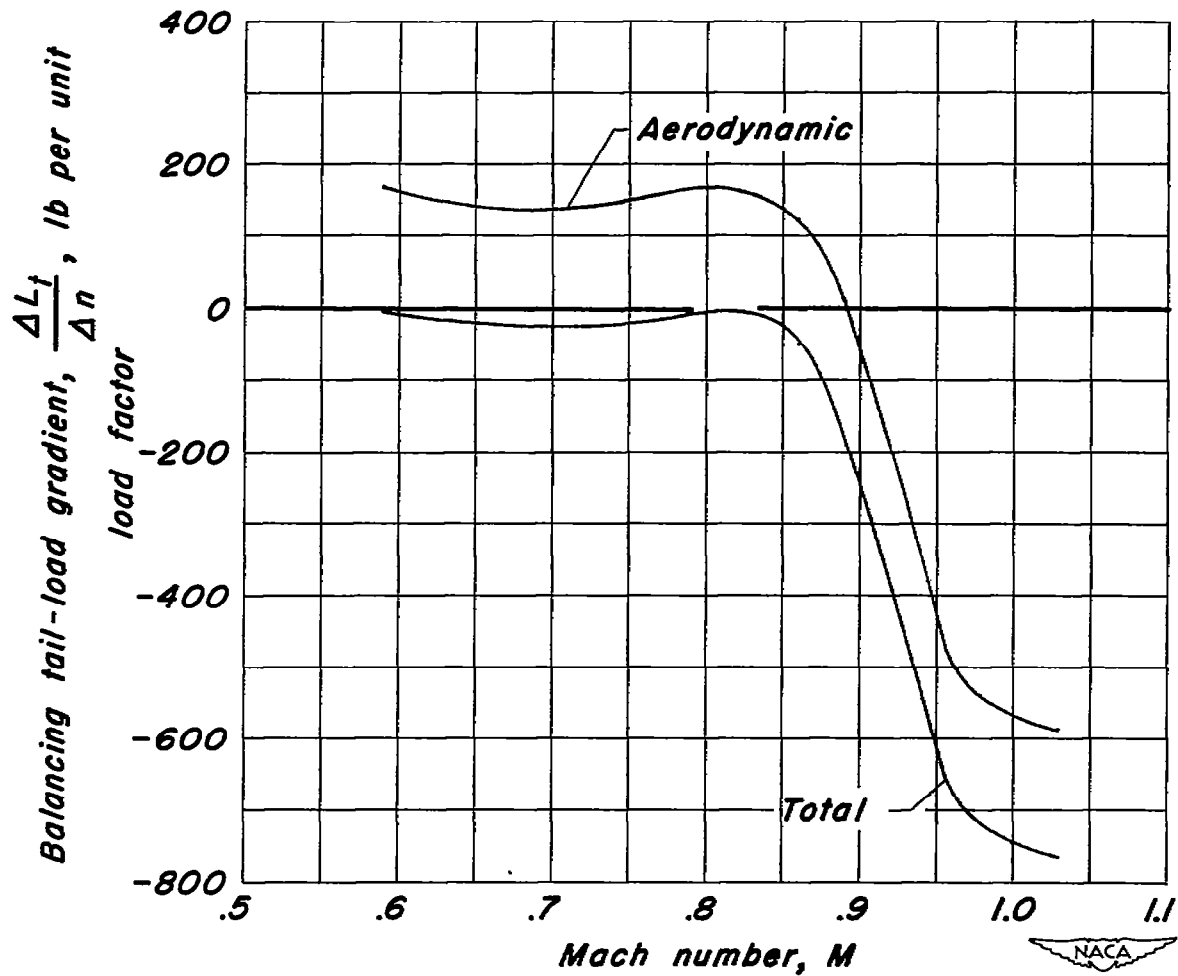


Figure 10. Variation with Mach number of the balancing tail-load gradients in gradual maneuvers up to the pitch-up region.

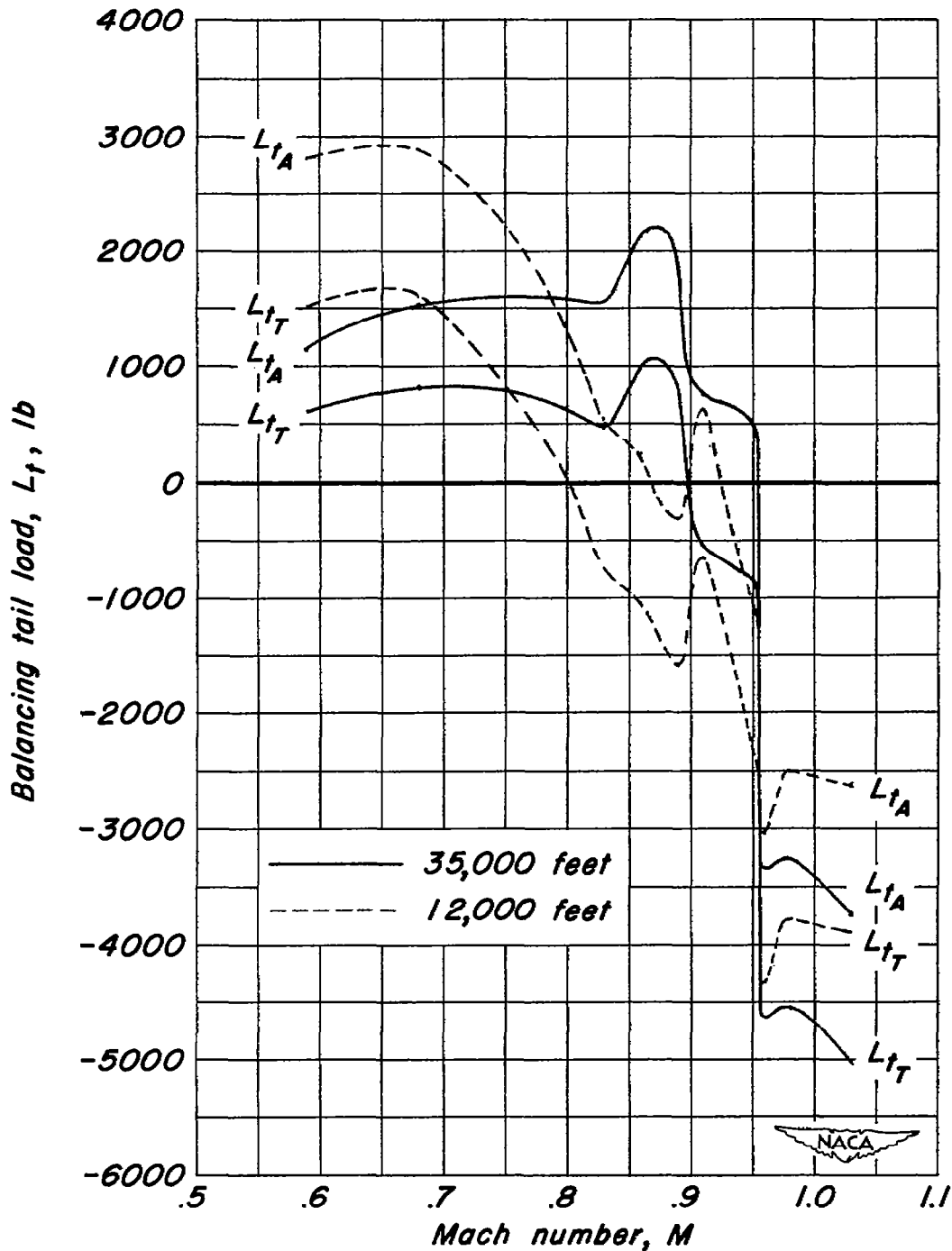


Figure 11.- Estimated limit balancing tail loads based on an extrapolation of the experimental results to design conditions at 35,000 feet and 12,000 feet. Center of gravity, 22.5-percent  $\bar{c}$ .

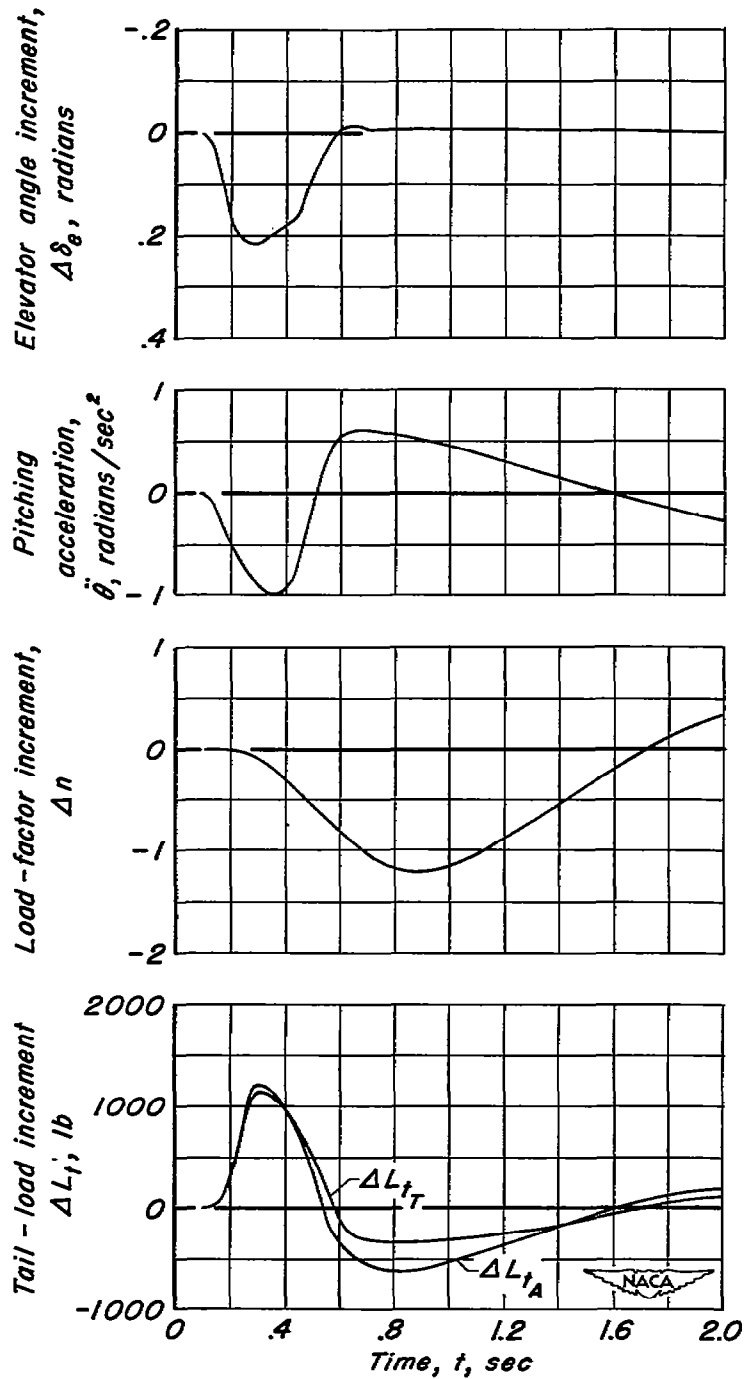
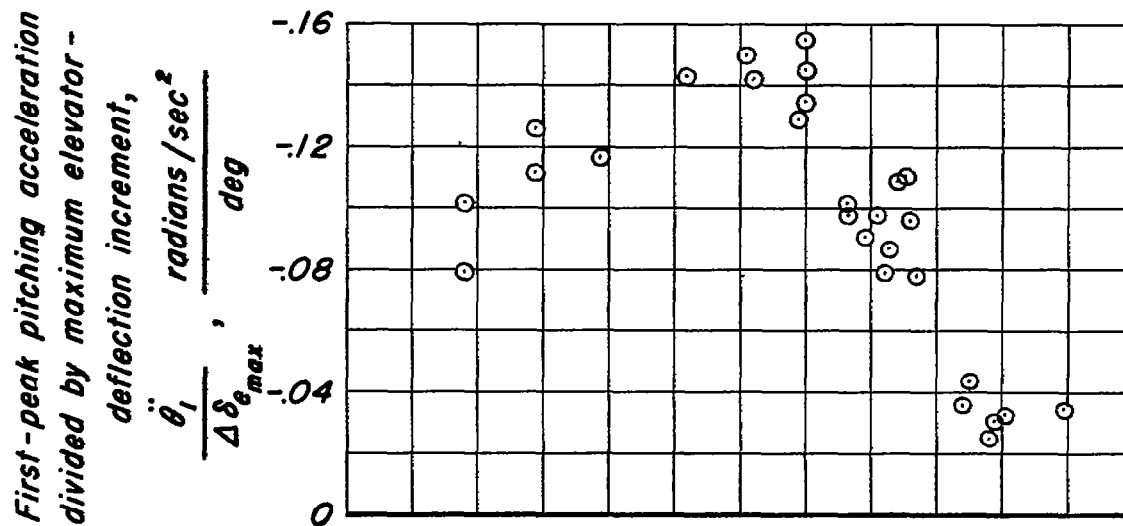
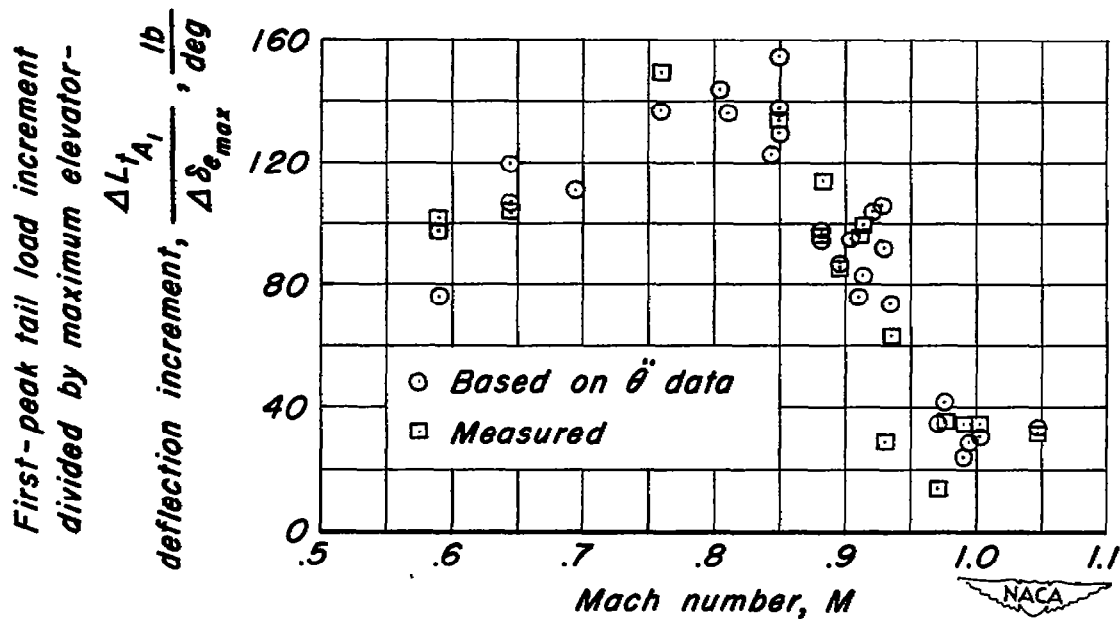


Figure 12.- Time history of airplane response to an elevator pulse at a Mach number of 0.59.



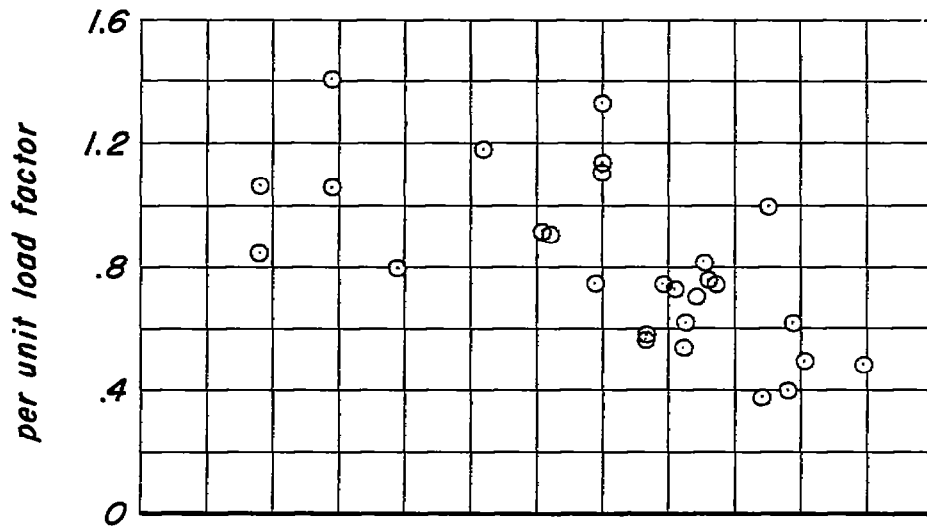
(a) Pitching acceleration.



(b) Tail load.

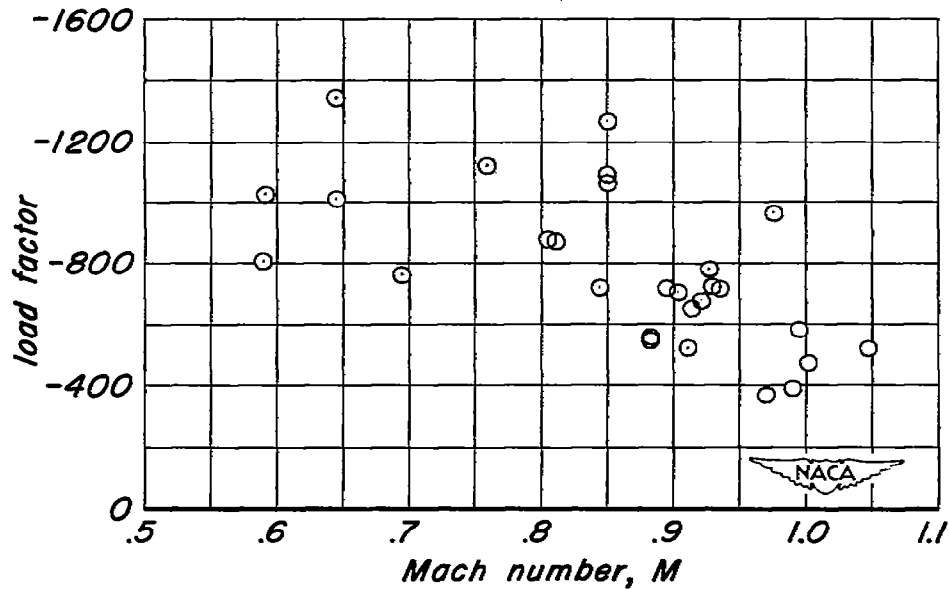
Figure 13.- Variation with Mach number of the first-peak pitching acceleration and tail load for a unit increment in maximum elevator deflection for the elevator-pulse maneuvers.

First-peak pitching acceleration  
divided by maximum load-factor  
increment,  $\frac{\ddot{\theta}_1}{\Delta n_{max}}$ , radians/sec<sup>2</sup>



(a) Pitching acceleration.

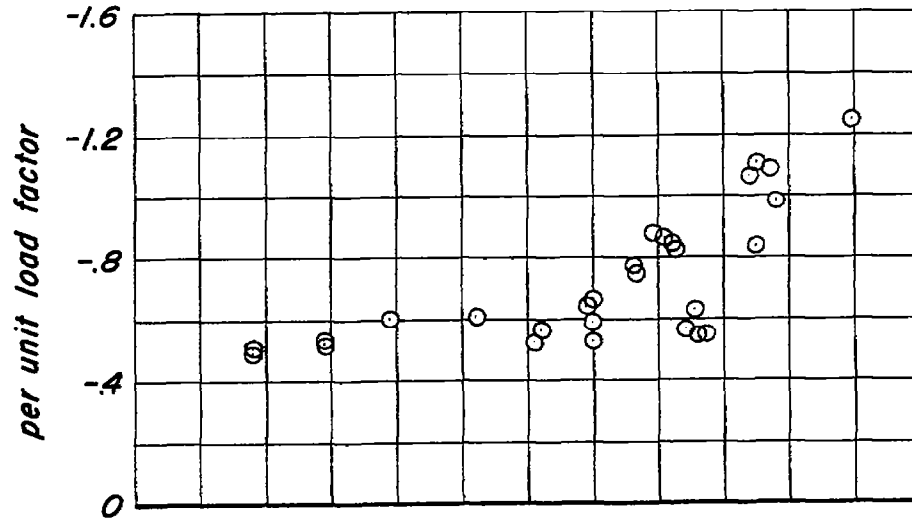
First-peak tail-load increment  
divided by maximum load factor  
increment,  $\frac{\Delta L_{tA_1}}{\Delta n_{max}}$ , lb per unit



(b) Tail load.

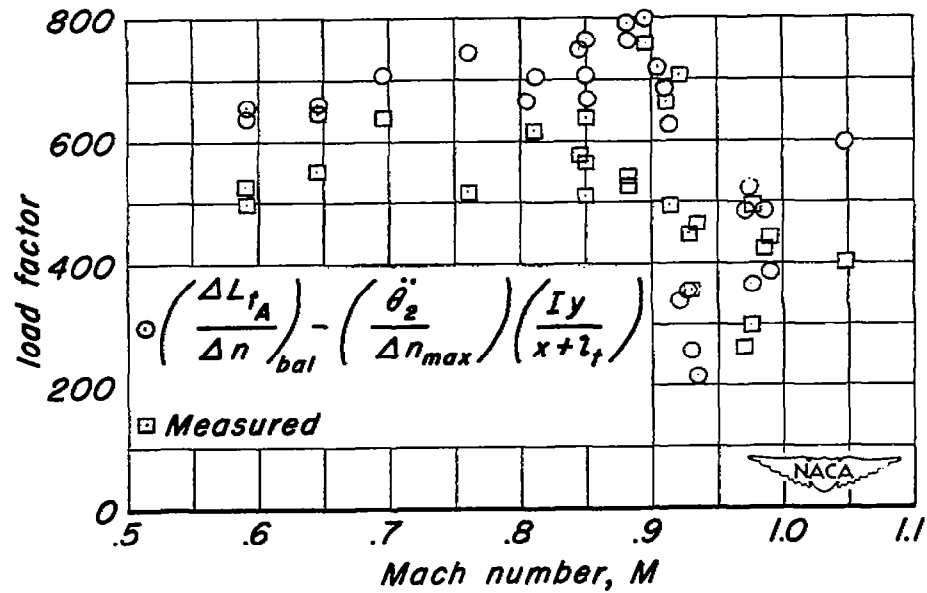
Figure 14.- Variation with Mach number of the first-peak pitching acceleration and tail load for a unit increment in maximum load factor for the elevator-pulse maneuvers.

Second-peak pitching acceleration  
divided by maximum load-factor  
increment,  $\frac{\ddot{\theta}_2}{\Delta n_{max}}$ , radians/sec<sup>2</sup>



(a) Pitching acceleration.

Second-peak tail-load increment  
divided by maximum load-factor  
increment,  $\frac{\Delta L_{tA_2}}{\Delta n_{max}}$ , lb per unit



(b) Tail load.

Figure 15.- Variation with Mach number of the second-peak pitching acceleration and tail load for a unit increment in maximum load factor for the elevator-pulse maneuvers.

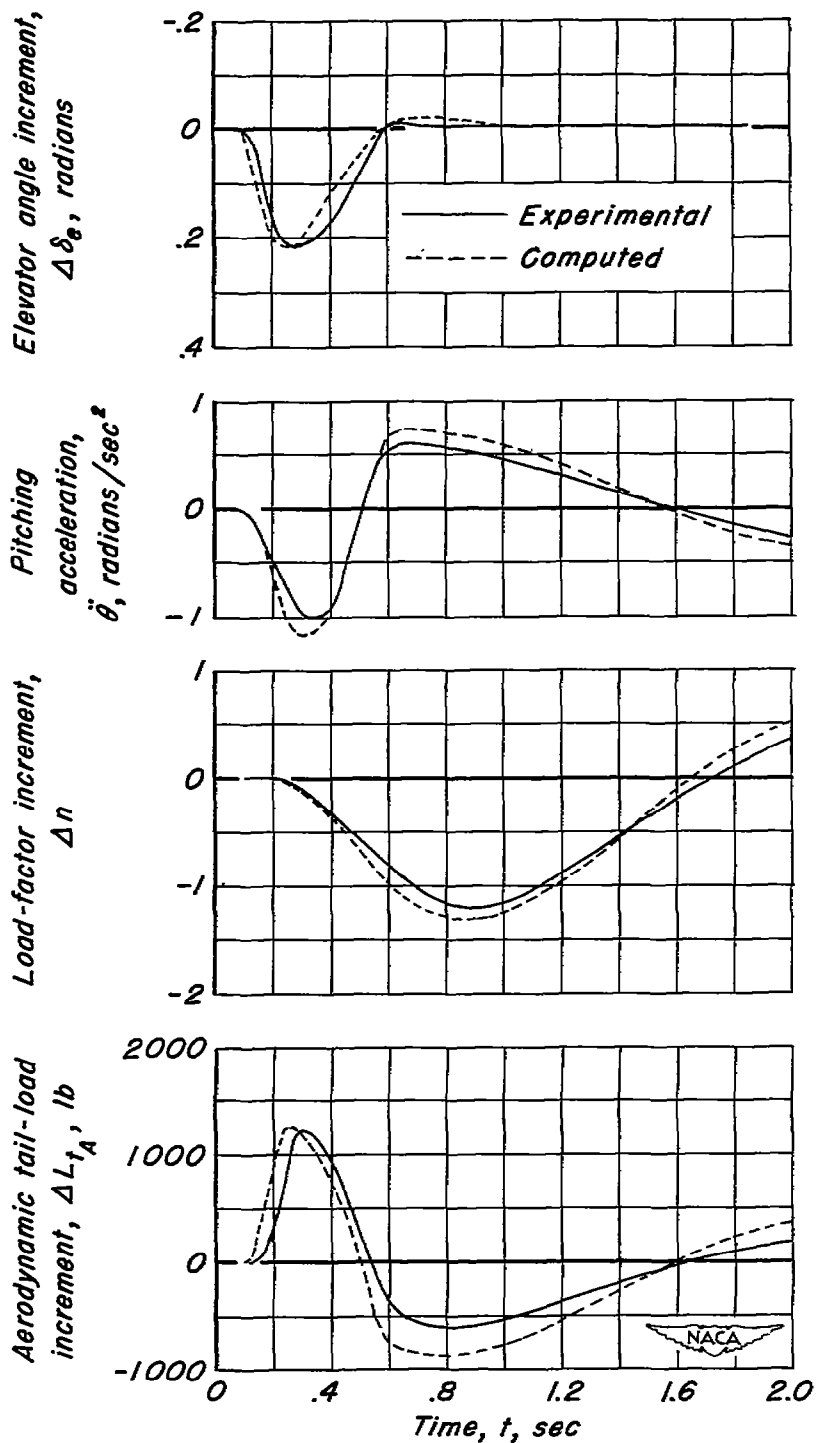
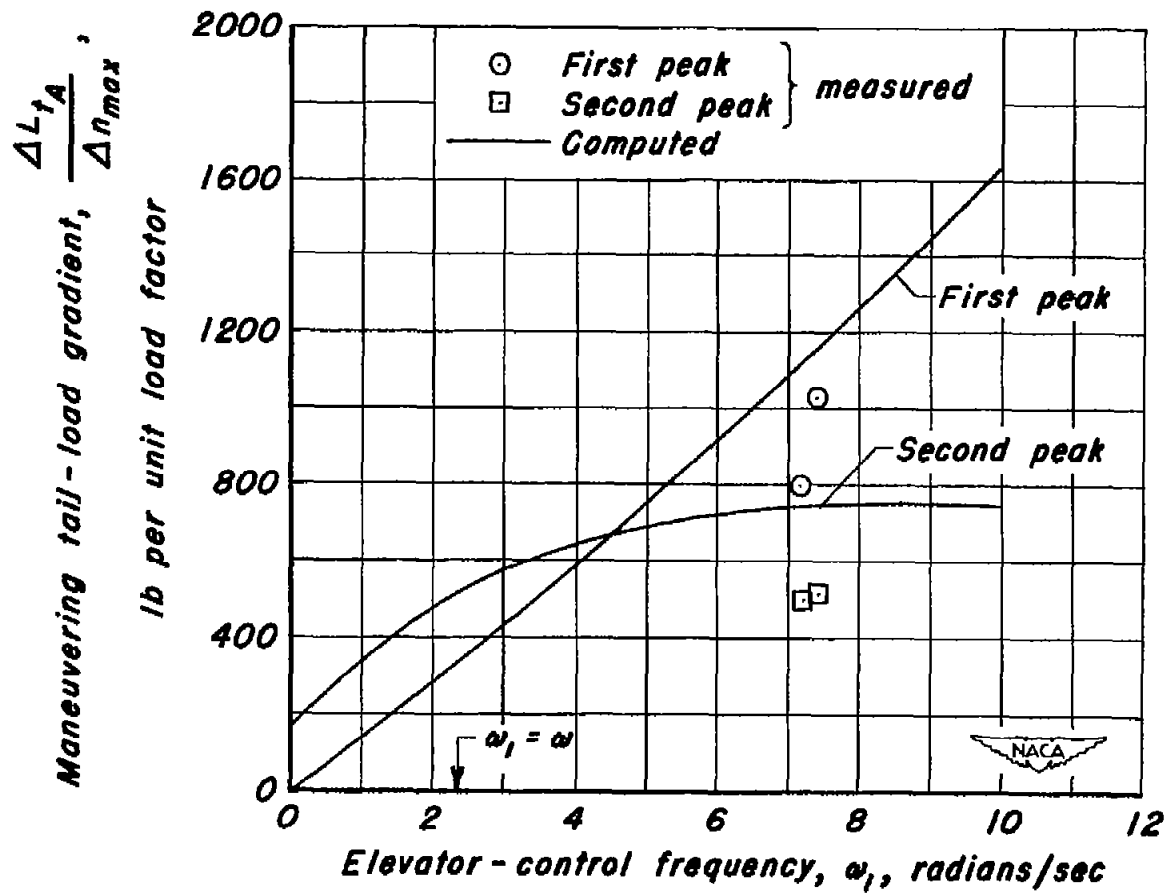
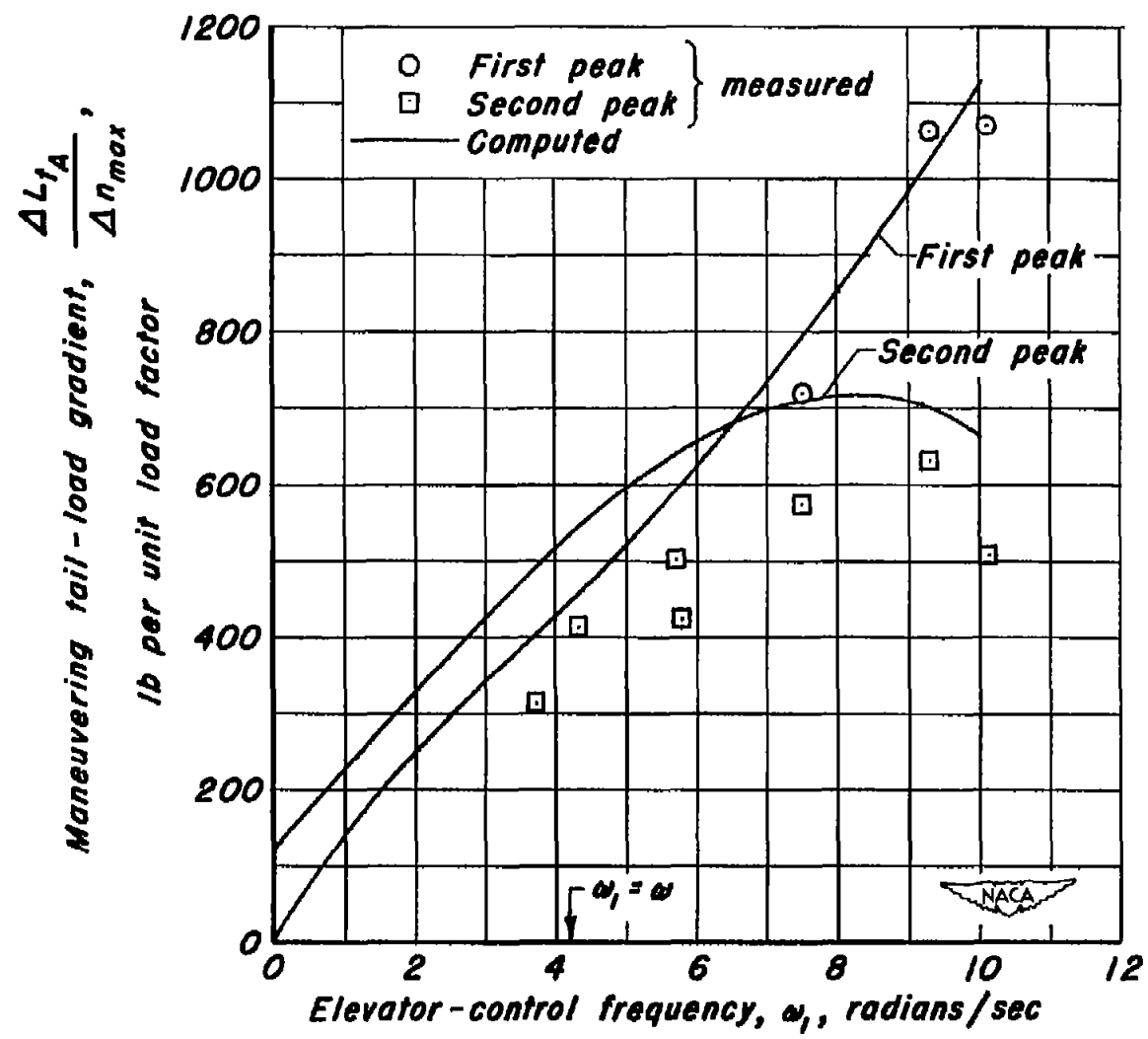


Figure 16.- Comparison between experimental and computed airplane response to an elevator pulse at a Mach number of 0.59.



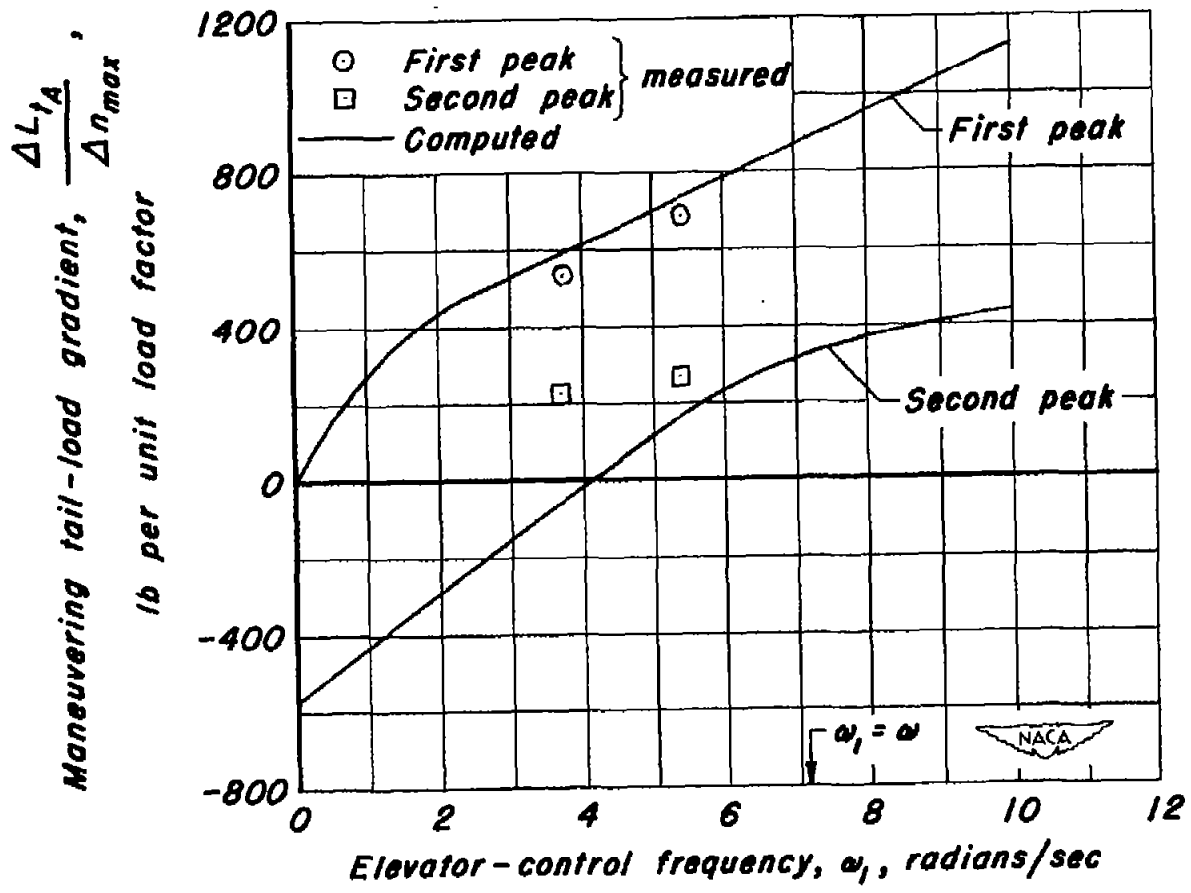
(a)  $M = 0.59$ ;  $\omega = 2.34$ .

Figure 17.-- Comparison between flight and computed maneuvering tail-load gradients at several values of elevator-control frequency.



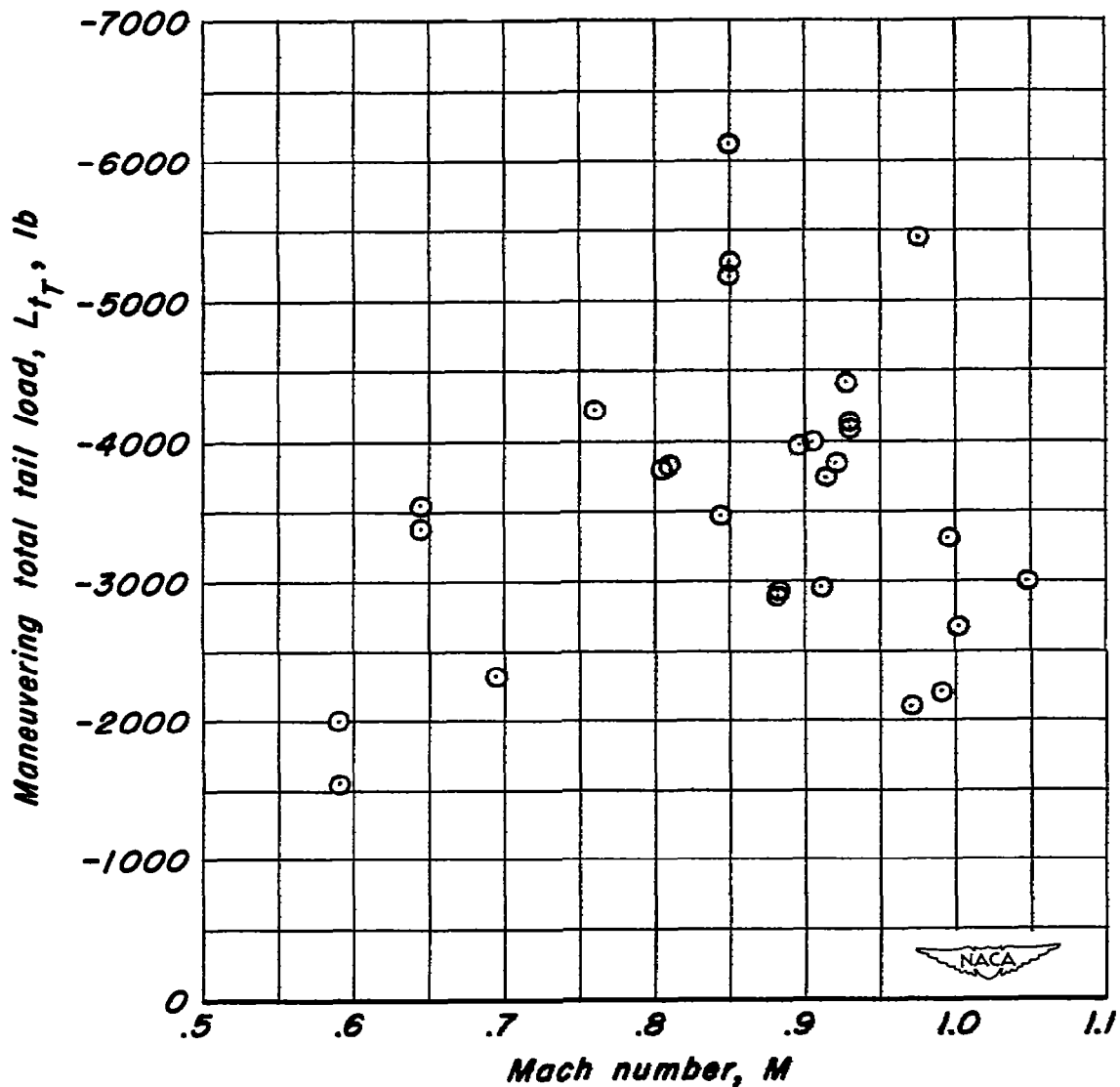
(b)  $M = 0.85$ ;  $\omega = 4.18$ .

Figure 17.- Continued.



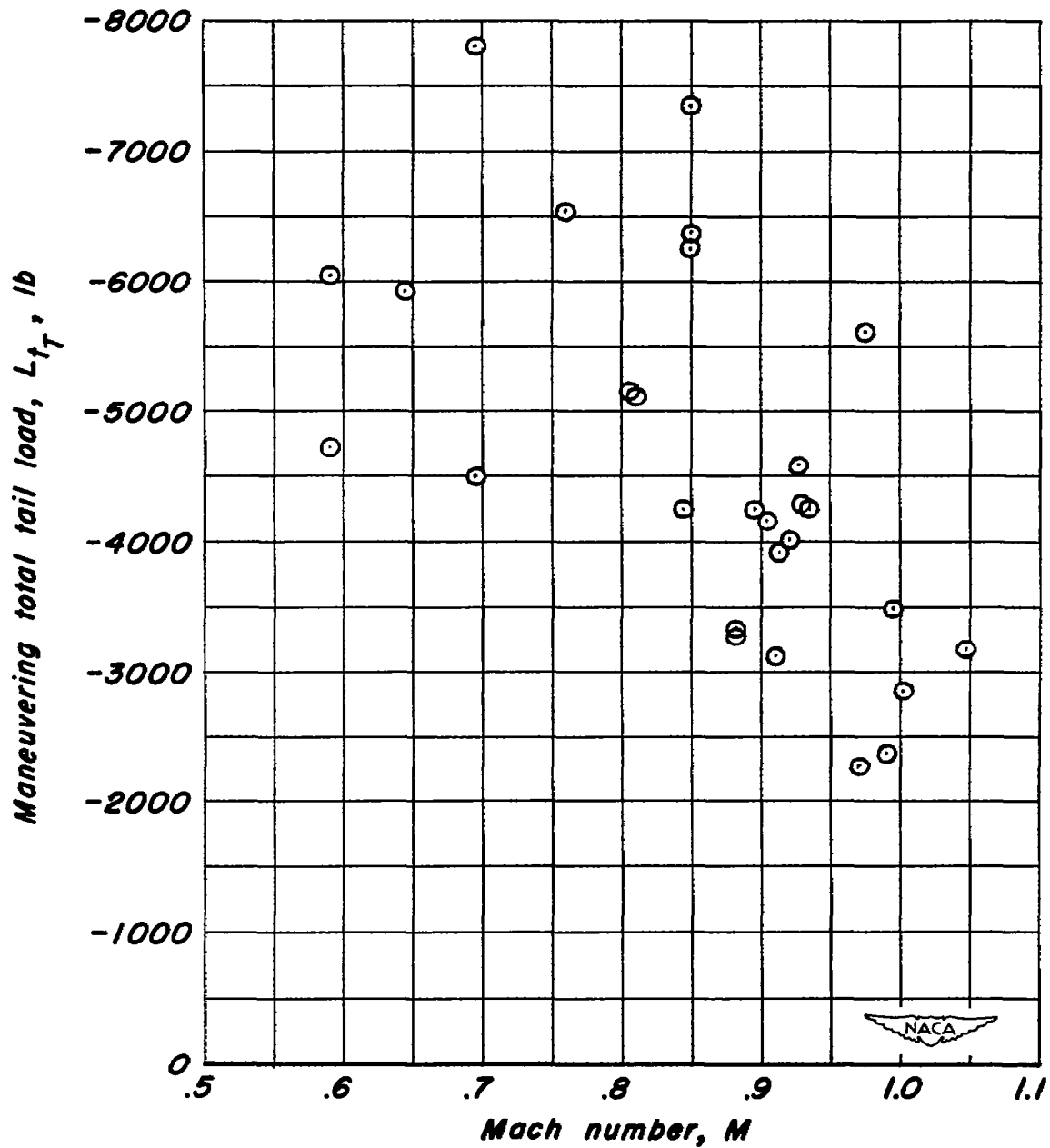
(c)  $M = 1.00$ ;  $\omega = 7.14$ .

Figure 17.- Concluded.



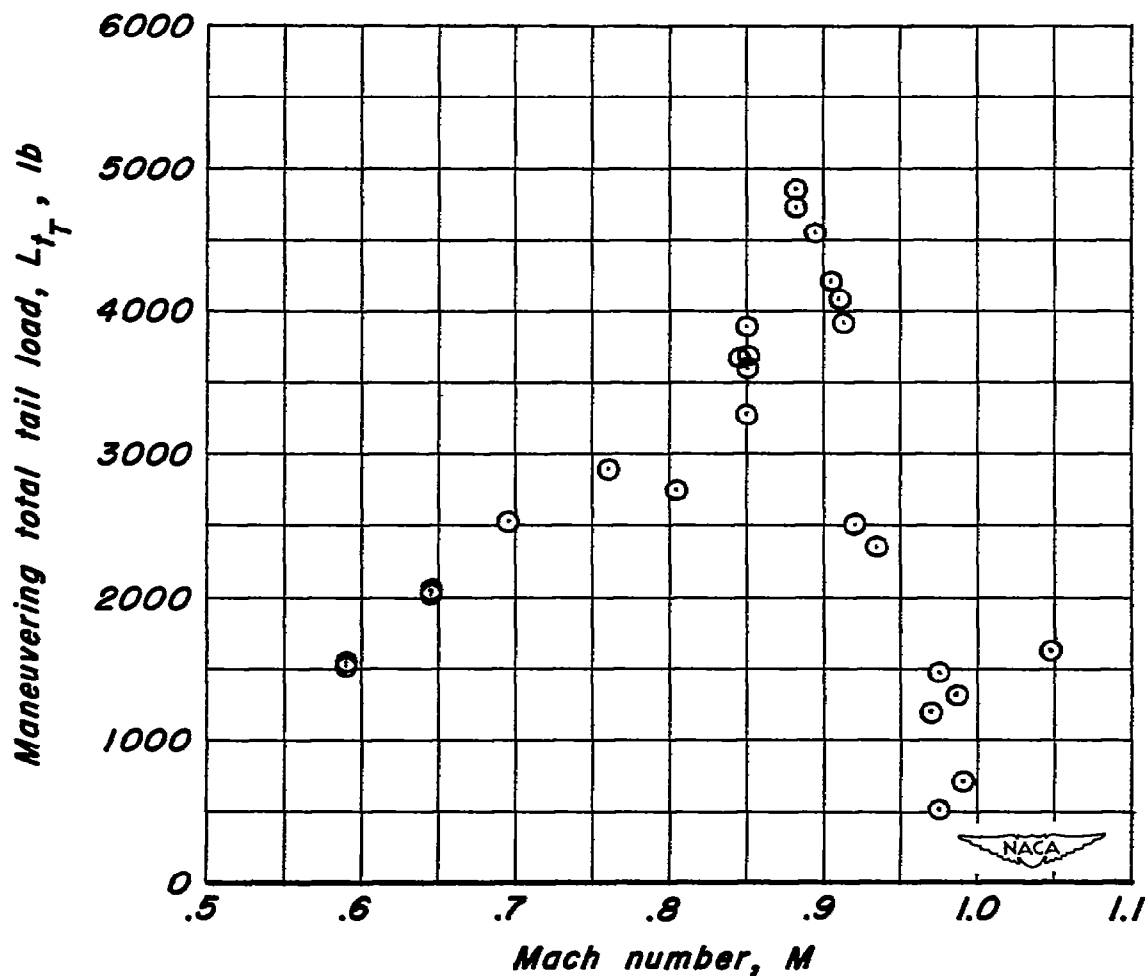
(a) 35,000 feet.

Figure 18.- Estimated limit first-peak total maneuvering tail loads based on an extrapolation of the experimental data to design conditions at 35,000 feet and 12,000 feet.



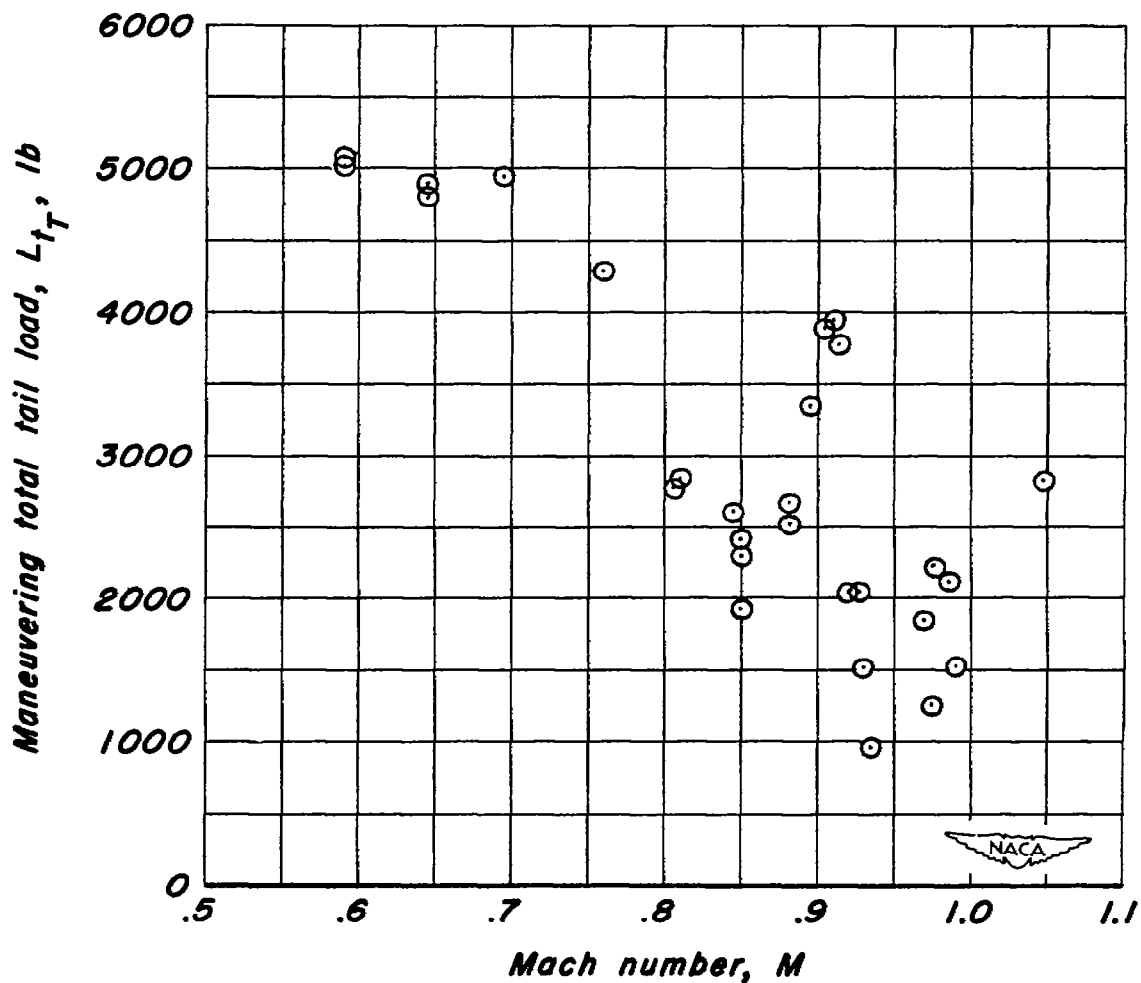
(b) 12,000 feet.

Figure 18.- Concluded.



(a) 35,000 feet.

Figure 19.- Estimated limit second-peak total maneuvering tail loads based on an extrapolation of the experimental data to design conditions at 35,000 feet and 12,000 feet.



(b) 12,000 feet.

Figure 19.- Concluded.

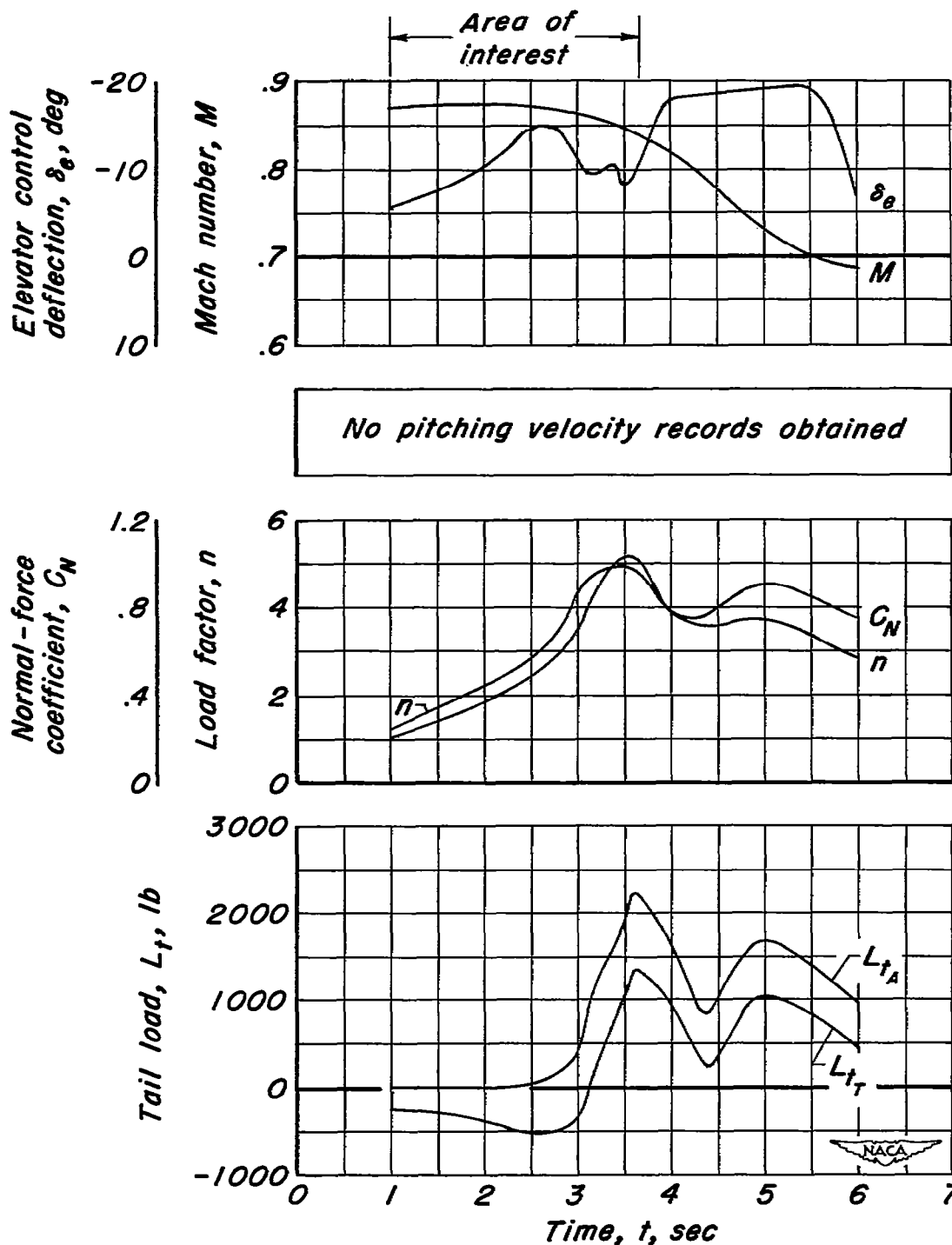


Figure 20.- Time history of a pitch-up maneuver initiated by a decrease in wing-fuselage stability with an increase in load factor at constant Mach number.

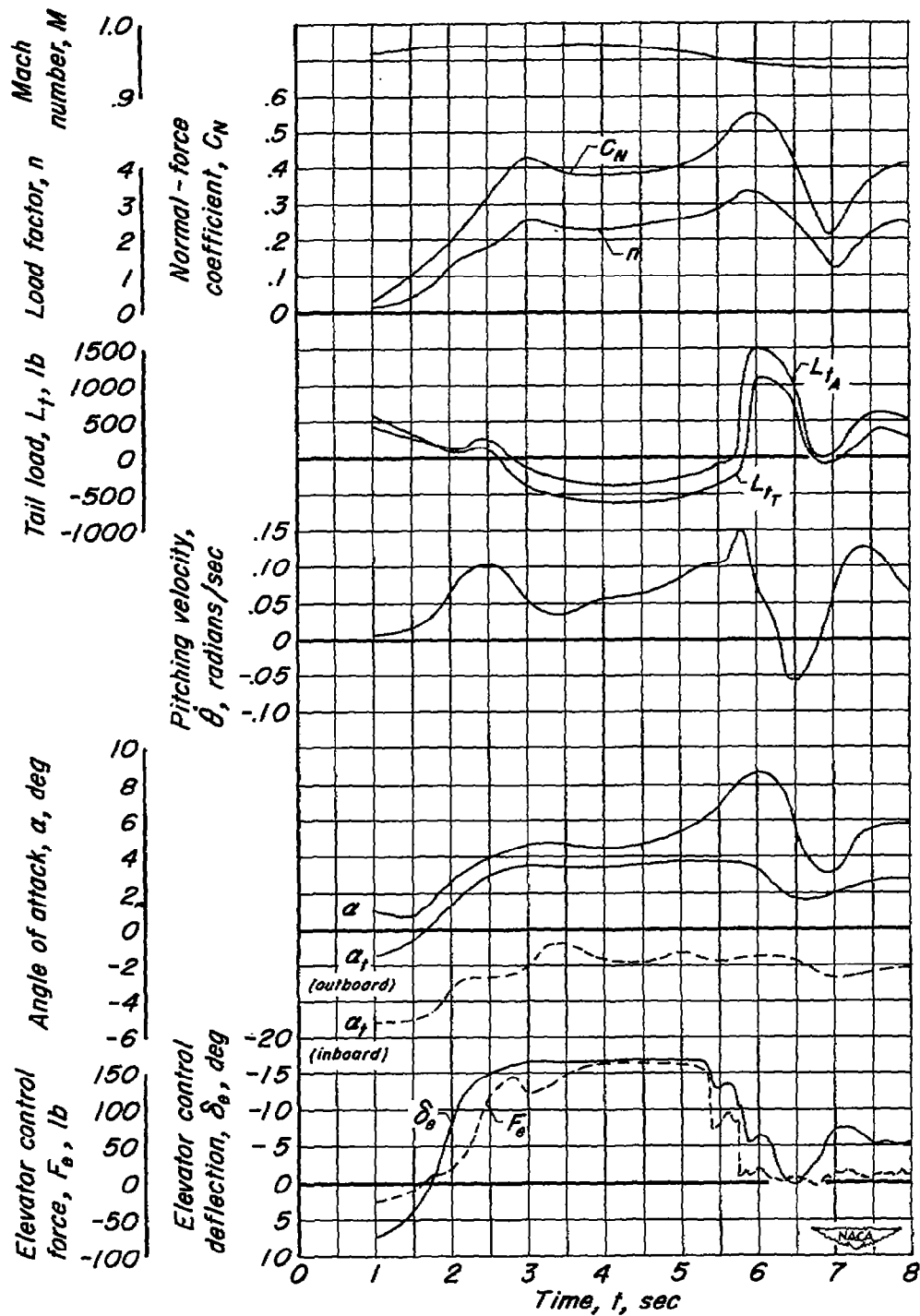


Figure 21.- Time history of a pitch-up initiated by a decrease in wing-fuselage stability with a decrease in Mach number at constant load factor.

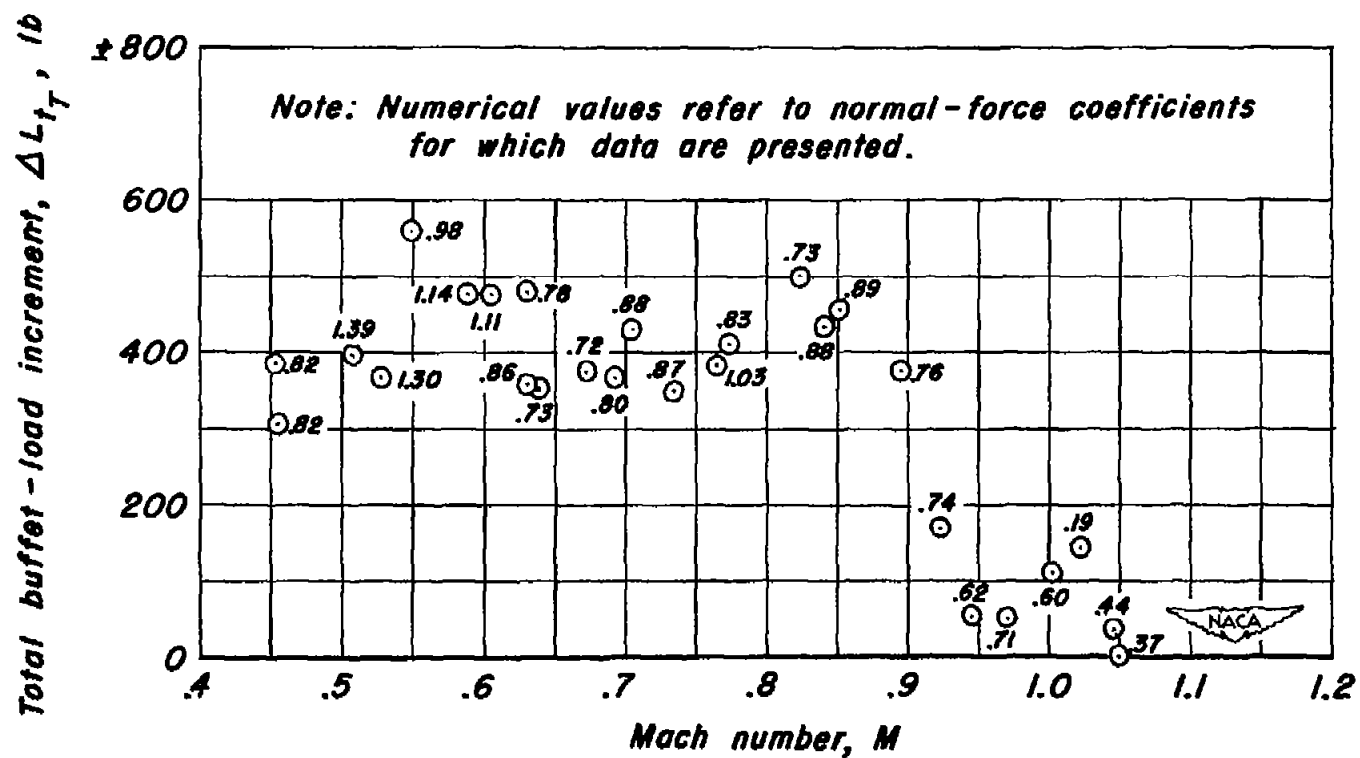


Figure 23.- Variation with Mach number of the maximum total buffet tail-load increments.

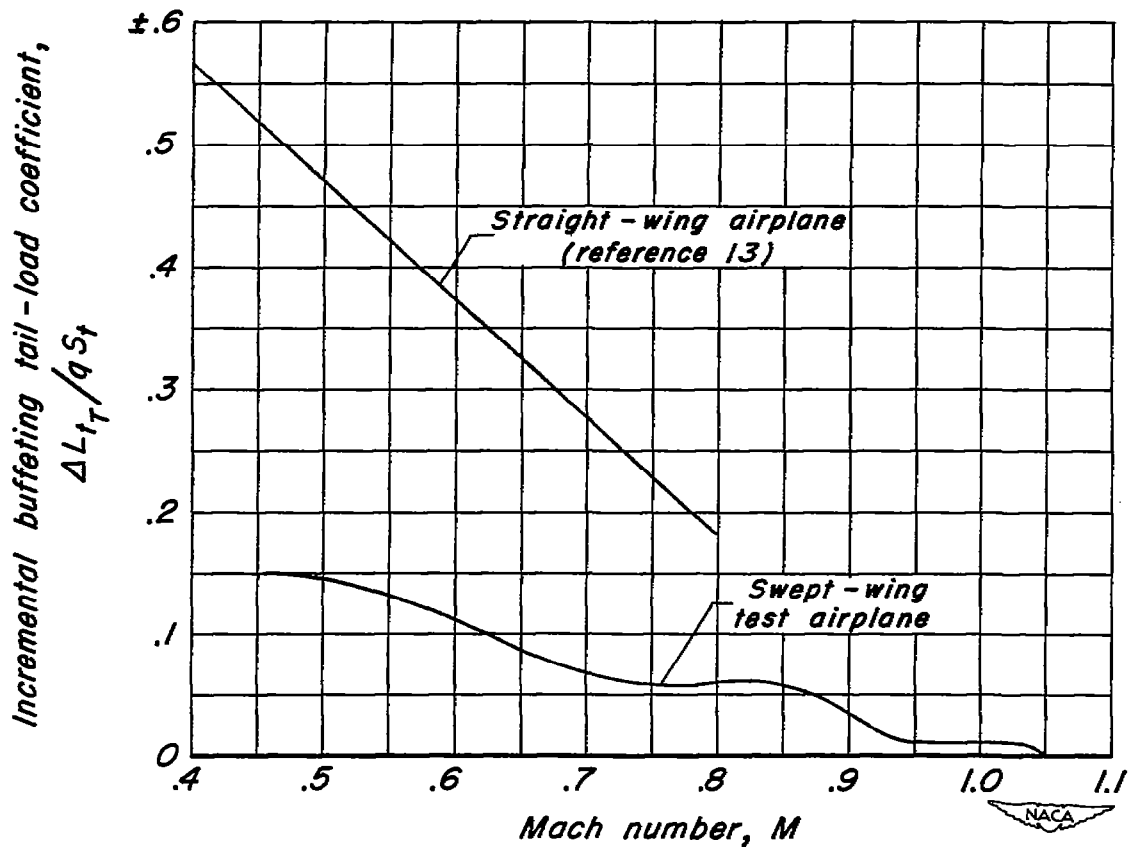


Figure 24.- Variation of maximum incremental buffeting tail-load coefficient with Mach number for the test airplane and a comparison with similar results for a straight-wing airplane.

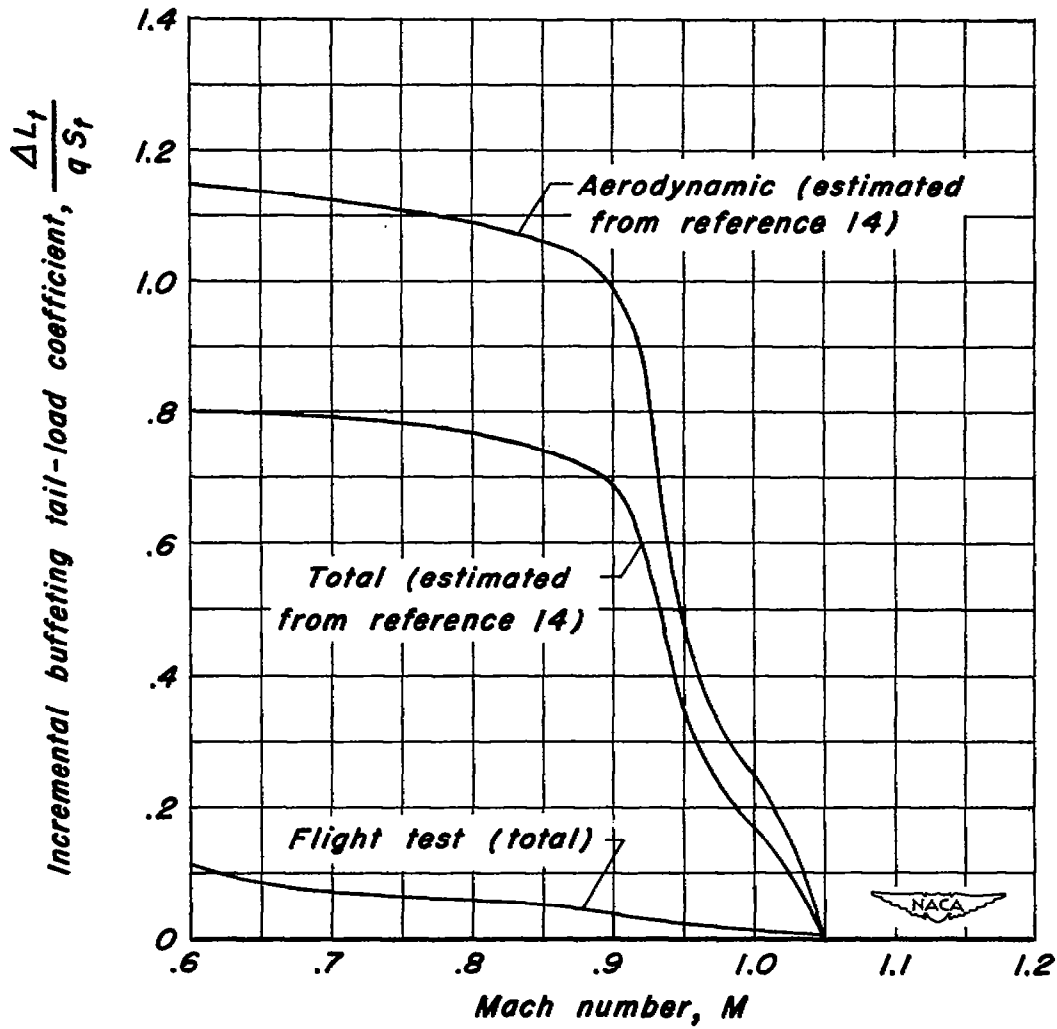


Figure 25.- Comparison between experimental and estimated incremental buffeting tail-load coefficients.

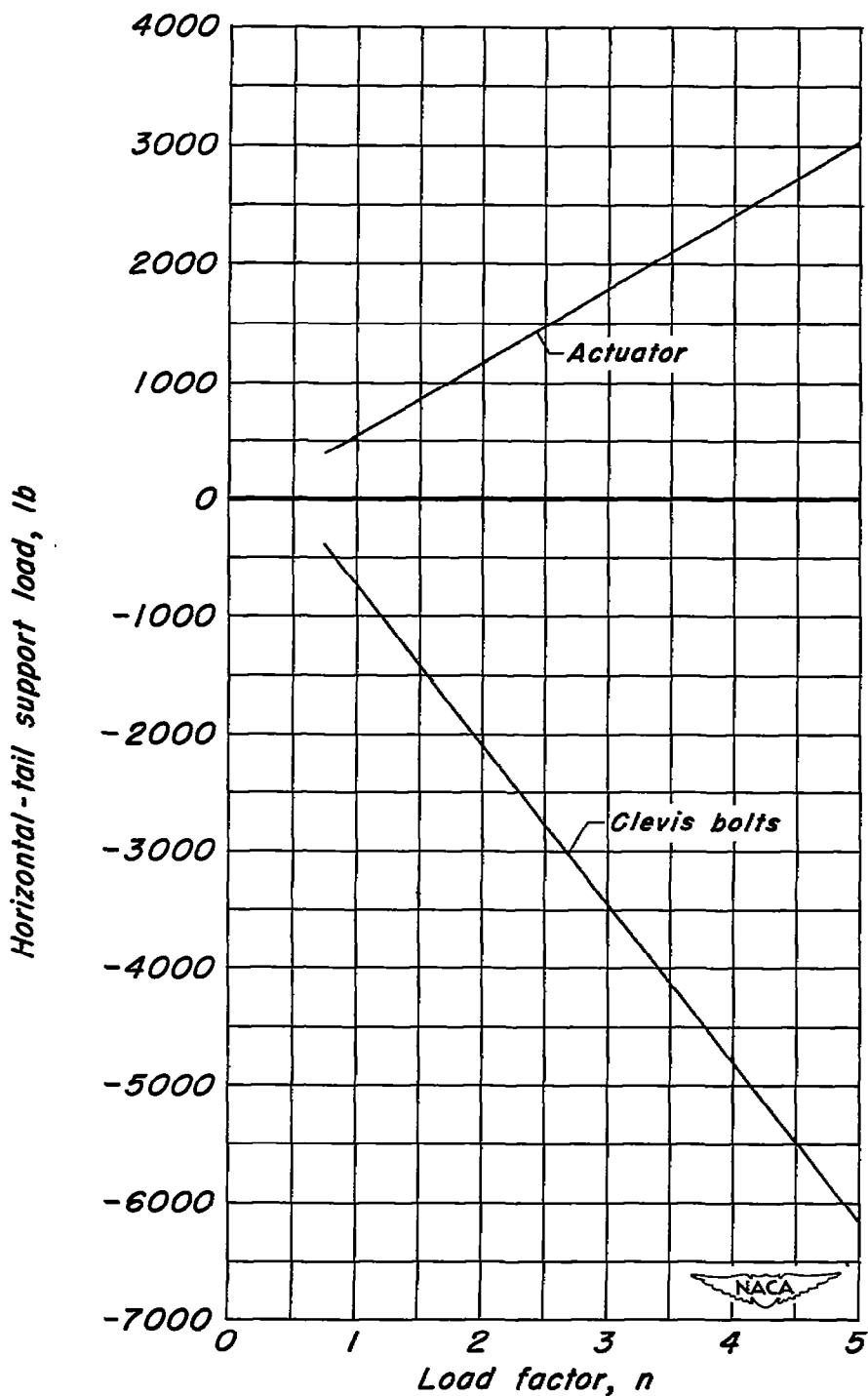


Figure 26.- Horizontal-tail support loads at critical flight region for total balancing tail loads.  $M \approx 1.0$ .

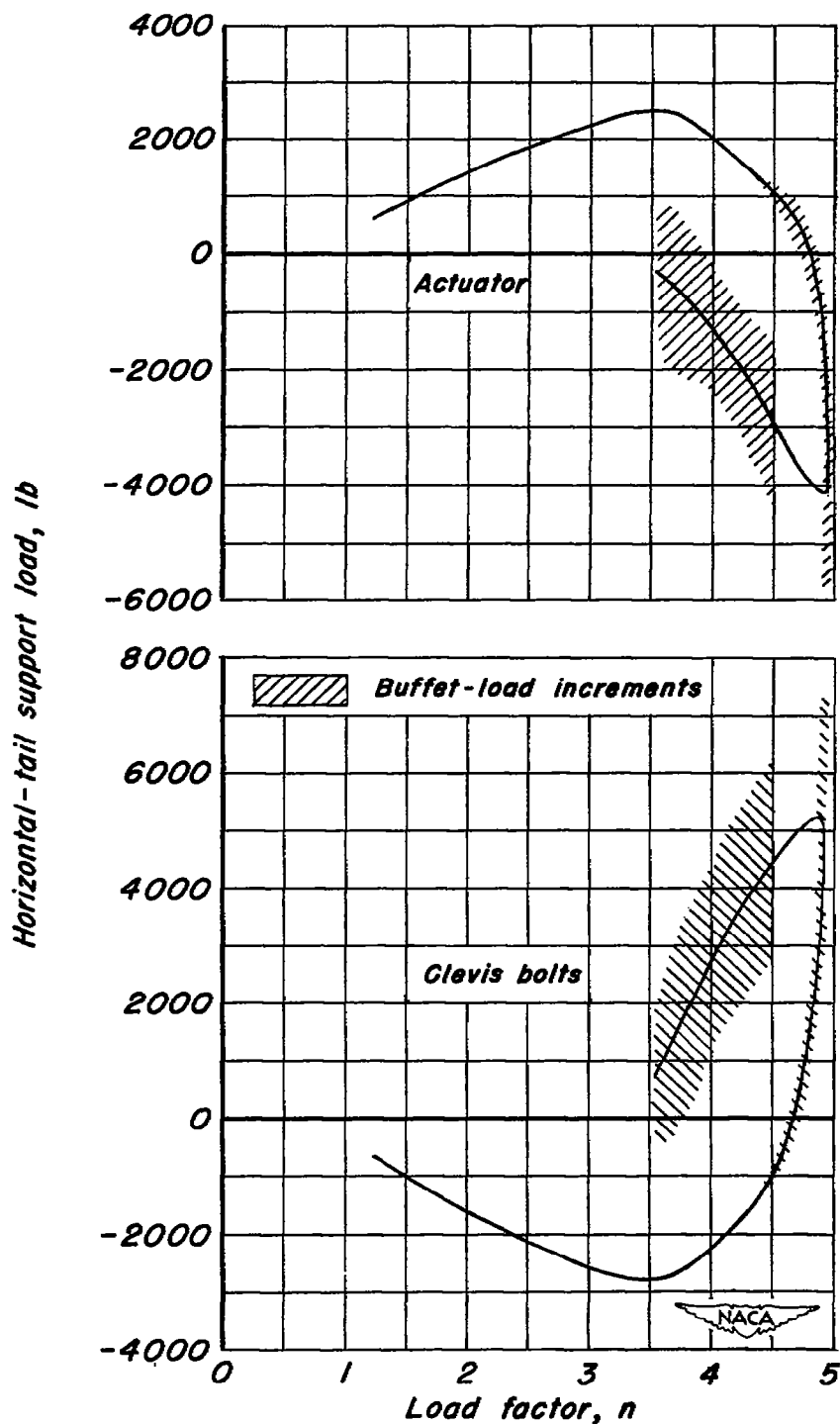
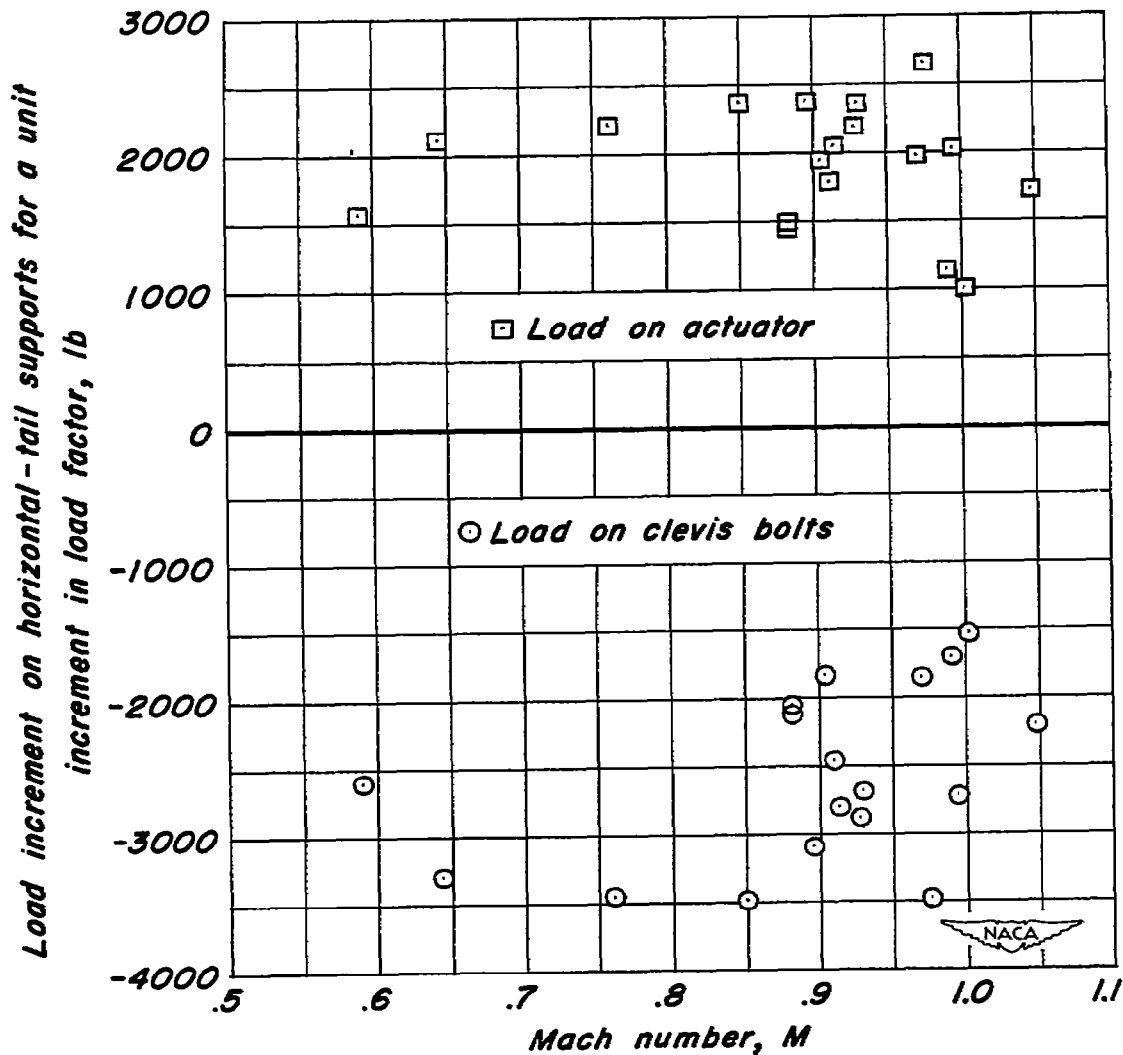
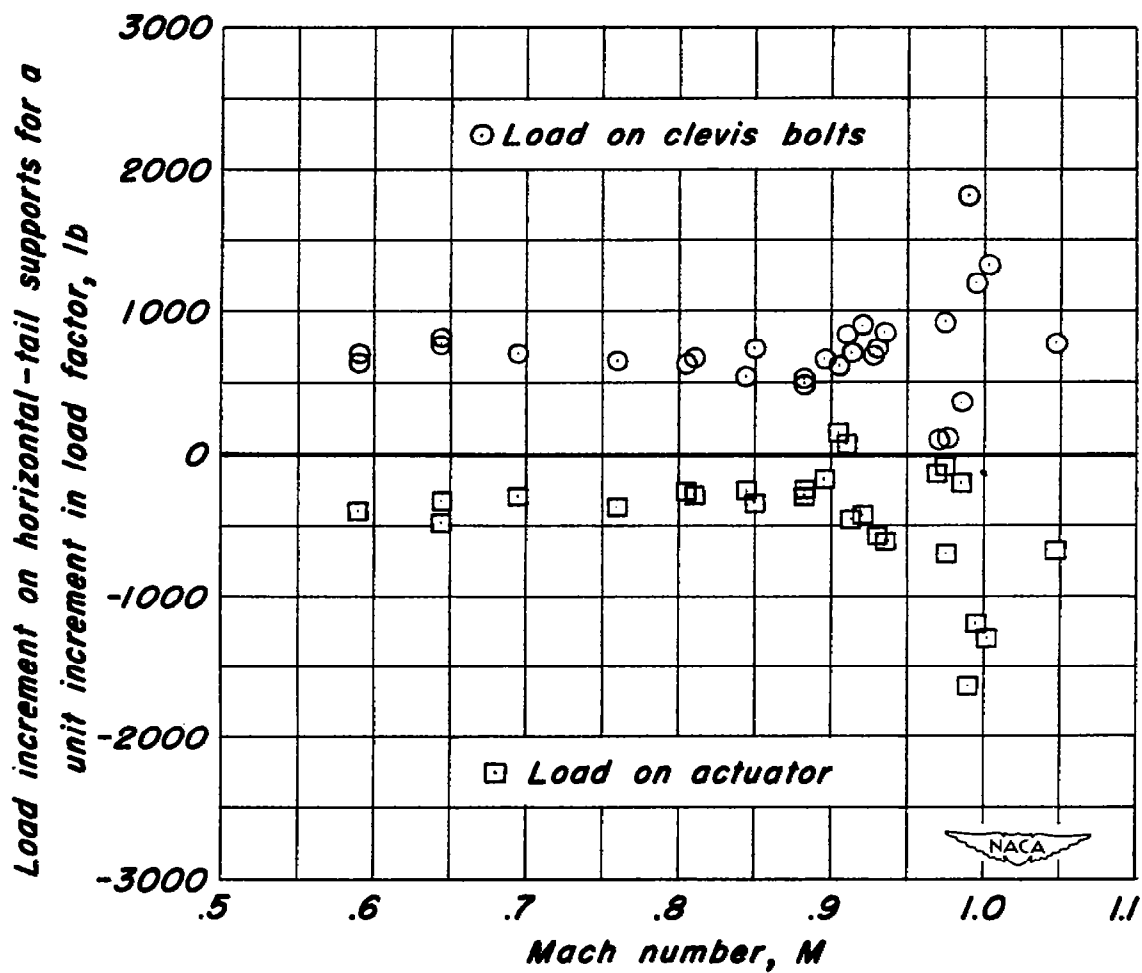


Figure 27.- Critical horizontal-tail support loads in a pitch-up initiated by wing-fuselage stability changes at constant Mach number.



(a) First-peak loads.

Figure 28.- Horizontal-tail support loads for a unit increment in load factor in abrupt elevator-pulse maneuvers.



(b) Second-peak loads.

Figure 28.- Concluded.

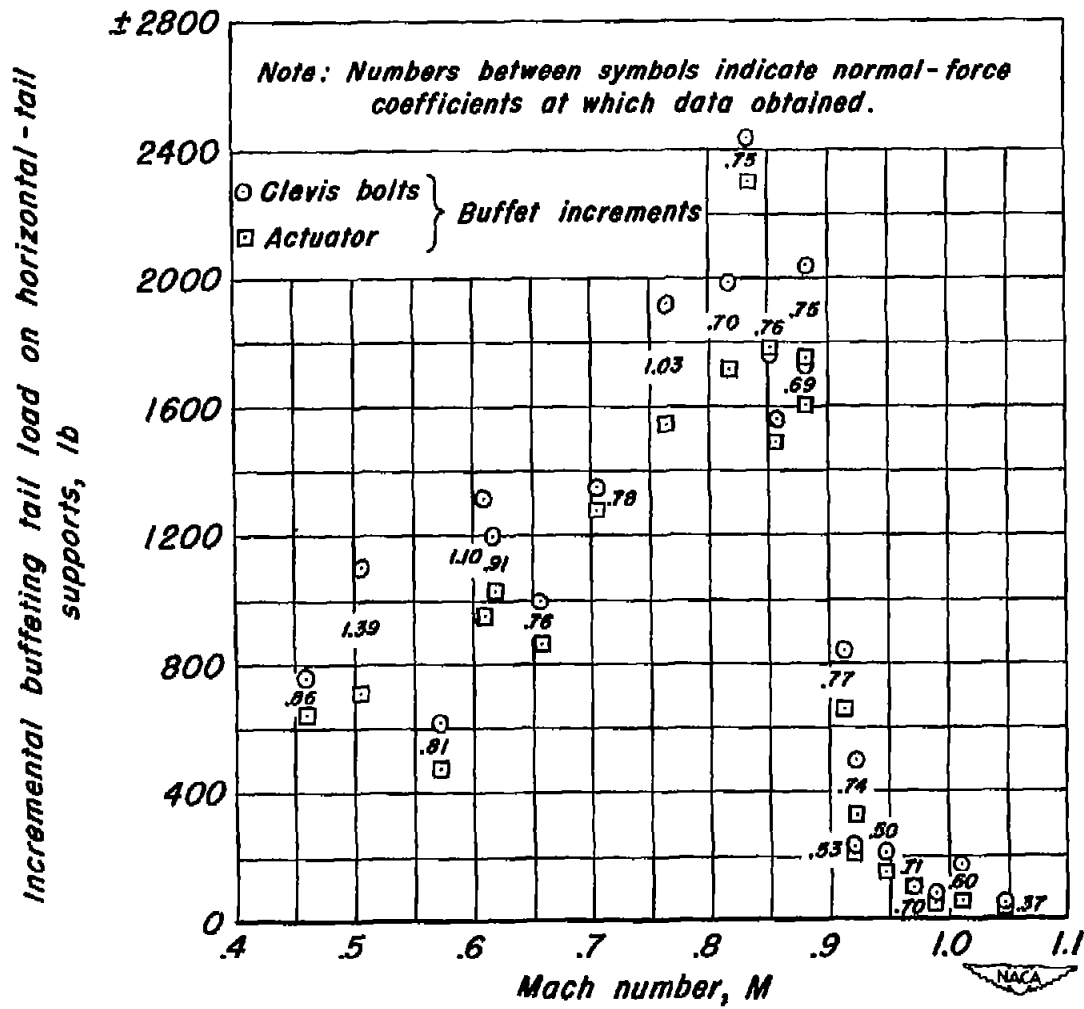


Figure 29.- Critical horizontal-tail support loads due to maximum buffet-load increments.

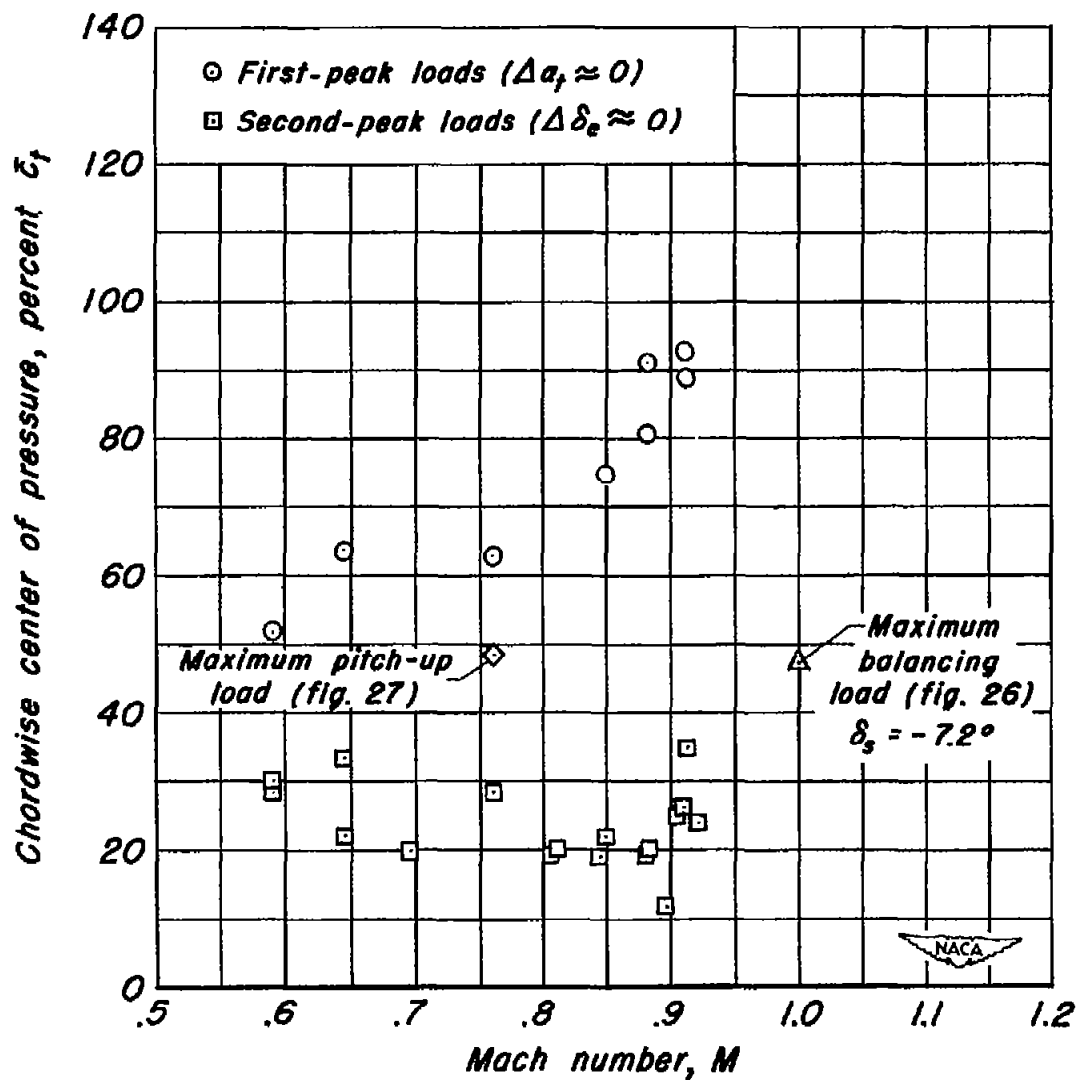


Figure 30.- Chordwise center-of-pressure data for several loading conditions.

SECURITY INFORMATION

~~CONFIDENTIAL~~

NASA Technical Library  
  
3 1176 01434 8024

~~CONFIDENTIAL~~